JGR Atmospheres

RESEARCH ARTICLE
10.1029/2019JD031087

Special Section:
A NEW ERA OF LIGHTNING OBSERVATIONS FROM SPACE

# Changes to the Appearance of Optical Lightning Flashes Observed From Space According to Thunderstorm Organization and Structure

**Michael Peterson**[1], **Scott Rudlosky**[2], **and Daile Zhang**[3]

[1]ISR-2, Los Alamos National Laboratory, Los Alamos, NM, USA, [2]NESDIS, STAR, SCSB, College Park, Maryland, [3]Earth System Science Interdisciplinary Center/Cooperative Institute for Climate and Satellites-Maryland, University of Maryland, College Park, MD, USA

**Key Points:**
- Changes in thunderstorm cloud/precipitation structure drive variations in optical flash characteristics
- Large stationary flashes are frequently observed near storm edges, while propagating flashes occur in stratiform rain regions
- Lightning "superbolts" are not just one type of lightning but can arise when flashes occur near storm edges or in stratiform flashes

**Supporting Information:**
- Supporting Information S1
- Movie S1

**Correspondence to:**
M. Peterson,
mpeterson@lanl.gov

**Citation:**
Peterson, M., Rudlosky, S., & Zhang, D. (2020). Changes to the appearance of optical lightning flashes observed from space according to thunderstorm organization and structure. *Journal of Geophysical Research: Atmospheres*, *125*, e2019JD031087. https://doi.org/10.1029/2019JD031087

Received 28 MAY 2019
Accepted 29 JAN 2020
Accepted article online 3 FEB 2020

**Abstract** Optical lightning observations from space reveal a wide range of flash structure. Lightning imagers such as the Geostationary Lightning Mapper and Lightning Imaging Sensor measure flash appearance by recording transient changes in cloud top illumination. The spatial and temporal optical energy distributions reported by these instruments depend on the physical structure of the flash and the distribution of hydrometeors within the thundercloud that scatter and absorb the optical emissions. This study explores how flash appearance changes according to the scale and organization of the parent thunderstorms with a focus on mesoscale convective systems. Clouds near the storm edge are frequently illuminated by large optical flashes that remain stationary between groups. These flashes appear large because their emissions can reflect off the exposed surfaces of nearby clouds to reach the satellite. Large stationary flashes also occur in small isolated thunderstorms. Optical flashes that propagate horizontally, meanwhile, are most frequently observed in electrified stratiform regions where extensive layered charge structures promote lateral development. Highly radiant "superbolts" occur in two scenarios: embedded within raining stratiform regions or in nonraining boundary/anvil clouds where optical emissions can take a relatively clear path to the satellite.

**Plain Language Summary** Lightning occurs in all shapes and sizes. Often, it is the thunderstorm that determines how a lightning flash appears from space. Dense clouds can block light from escaping the cloud top with enough energy to be detected from orbit. Light also can reflect off lower cloud layers to make flashes appear larger than in reality. The size and organization of thunderstorms change as they grow, develop, and eventually dissipate. Changes in the clouds affect how the light produced by lightning is scattered, reflected, and observed. Combining measurements of clouds and lightning illustrates how lightning flash appearance may provide important insights into thunderstorm development.

## 1. Introduction

The structure of parent thunderstorms controls the physical nature of lightning and how its optical signals are modified on their way to orbit. Connections between the meteorological and electrical aspects of thunderstorms are complex and have motivated decades of physical research. Peterson, Deierling, et al. (2017) examined how the immediate cloud region surrounding the lightning flash modified its appearance. The present study moves upscale to explore how overall thunderstorm organization and structure influence the types of flashes produced. The following introductory sections present a basic overview of important mechanisms that influence observations from the Geostationary Lightning Mappers (GLM; Goodman et al., 2013) on the new R series Geostationary Operational Environmental Satellites (GOES). Early work with the Lightning Imaging Sensor (LIS; Blakeslee et al., 2014; Christian et al., 2000) also helps establish the necessary groundwork for our new results. GLM will be used to explore thunderstorm evolution over time, while LIS on the Tropical Rainfall Measuring Mission satellite (TRMM; Kummerow et al., 1998) will be used to examine lightning in the context of the precipitation structure of the surrounding thunderstorm.

### 1.1. Connections Between Thunderstorm Precipitation and Electrical Structures

For lightning to occur, sufficiently strong electric fields within the storm must overcome the electrical impedance of the air. A leading theory on thunderstorm electrification is the noninductive charging mechanism (Bruning et al., 2014; Jayaratne et al., 1983; Mansell et al., 2005; Reynolds et al., 1957; Saunders et al., 1991;

Saunders & Peck, 1998; Takahashi, 1978; Takahashi & Miyawaki, 2002). When large graupel pellets rimed with supercooled liquid water collide with smaller ice particles in a convective updraft, charge may be transferred from one species of ice to the other. Typically, this involves electrons being sheared off of the small ice particles and deposited onto the larger graupel pellets.

These charged hydrometeors are then organized by thunderstorm kinematics into the common precipitation structures measured by weather radars. For example, the updrafts in convective cells sort hydrometeors by mass, lofting the small ice particles that typically attain a positive charge toward the cloud top while leaving the larger (often negatively charged) graupel pellets in the midlevels of the storm. Over time, the accumulation of charged particles in these regions leads to a semipersistent thunderstorm charge structure. Williams (1989) described this charge structure using a tripole model that additionally includes a smaller positive charge region near the cloud base. Charge structures found in nature can be considerably more complex than simple models, however (e.g., Byers & Braham, 1949; Krehbiel, 1986; Rust et al., 2005; Stolzenburg et al., 1994; Stolzenburg et al., 1998), and they change as the thunderstorm evolves.

Deierling and Petersen (2008) showed that time series of total lightning activity—including both cloud-to-ground flashes and intracloud flashes—could be used to track changes in the thunderstorm updraft volume above the −5 °C isotherm. Deierling et al. (2008) demonstrated with dual-Doppler radar observations that estimated precipitation and nonprecipitation ice mass above the melting level correlates strongly with total lightning activity. Drastic changes in the total lightning flash rate from ground-based Lightning Mapping Array (LMA; Rison et al., 1999) networks have also been shown to precede the onset of severe weather such as tornadoes and hail. Lightning Jump Algorithms (Schultz et al., 2009, 2017) have been constructed to capitalize on this link between updraft evolution, lightning, and severe weather.

### 1.2. Influences of Thunderstorm Organization on Lightning Flash Structure

Lightning flash characteristics also respond to variations in thunderstorm microphysics and kinematics. Bruning and MacGorman (2013) describe the theoretical basis for lightning near strong updrafts having a higher flash rate but smaller overall size. They also provide observational evidence that this opposition between frequent breakdowns and large flash extents occurs in nature.

Large lightning flashes often extend into (or are initiated in) anvil (Kuhlman et al., 2009; Weiss et al., 2012) and stratiform regions (Carey et al., 2005) of the parent thunderstorm and interact with (or result from) local charge structures. Charged ice particles advected into stratiform and anvil clouds from the convective core can be enhanced by local in situ charging processes (Ely et al., 2008; Lang & Rutledge, 2008). These mechanisms produce vertically limited and often horizontally extensive charge layers within nonconvective clouds. Anvil clouds may have a single primary charge layer with opposite polarity screening layers at the cloud boundaries (Marshall et al., 1989) while stratiform clouds may contain up to six horizontally stacked charge layers on the order of 100 km across (Krehbiel, 1986; Lang et al., 2004; Marshall et al., 2009; Marshall & Rust, 1993; Stolzenburg et al., 1994).

Because lateral flash development is guided by potential wells (extrema in the local electric field profile) (Coleman et al., 2008), the layered charge structures that are set up in electrified anvil and stratiform clouds may act as conduits for horizontal flash propagation. This would explain why lightning flashes that interact with charge regions outside of the convective core often develop laterally over considerable horizontal distances. The World Meteorological Organization certified world records are currently held by LMA systems. The longest lasting lightning flash certified at the time of writing is 7.72 s from southern France, while the largest lightning flash by horizontal extent is 321 km from Oklahoma (Lang et al., 2017). Both of these world record flashes are cases where the lightning is initiated in the convective core and then propagates deep into the stratiform region. Expansive horizontal lightning has been observed from space since the Space Shuttle era (Vonnegut et al., 1985) and can be mapped by lightning imagers (Peterson et al., 2018). The lightning flashes with the most extensive horizontal development measured by LIS (Peterson, Rudlosky, et al., 2017) and GLM (Peterson, 2019a) are also exclusively cases of propagating stratiform flashes.

### 1.3. Influences of Thunderstorm Structure on Lightning Flash Appearance via Scattering

Direct interactions between the optical signals generated by lightning with the hydrometeors in the cloud layer also modify the appearance of lightning measured from orbit. Precipitation particles scatter the emitted optical radiance throughout the cloud volume (i.e., Light, Suszcynsky, Kirkland, et al., 2001). This scattering

introduces a time-of-arrival delay and a pulse width broadening in the optical waveforms recorded from orbit relative to the radio frequency signals from the same event (Koshak et al., 1994; Light, Suszcynsky, & Jacobson, 2001). Scattering and absorption can prevent optical detection entirely if the radiated energy must traverse a sufficiently dense cloud layer (Thomson & Krider, 1982). Thomas et al. (2000) determined that the optical lightning signals that are detected from orbit tend to originate in the upper portion of the cloud. Emissions sources that are confined to low to middle levels are less readily detected from space, and the recorded signals tend to occur relatively late in the discharge. Scattering encourages optical lightning emissions to escape the sides of thunderclouds and illuminate the tops and sides of neighboring clouds, which in turn makes flashes appear larger than in reality (Peterson, Deierling, et al., 2017). Comparing GLM measurements of cloud top illumination with idealized solutions assuming a homogeneous cloud medium reveals contrasts in radiant energy indicative of hail cores, reflections, and flashes with long horizontal channels (Peterson, 2019b).

### 1.4. Variations in Flash Appearance With Thunderstorm Organization and Structure

The organization and cloud/precipitation structure of the parent thunderstorm influences the appearance of LIS and GLM lightning flashes through their established charge structures and by modifying optical lightning emissions through scattering and absorption. The present study uses thunderstorm snapshots from the TRMM satellite to establish statistical relationships linking the precipitation structure of thunderstorms with the characteristics of the lightning flashes they produce. We then examine whether these trends agree with continuous joint GLM and Advanced Baseline Imager (ABI; Schmit et al., 2017, 2018) measurements of a single long-lived mesoscale storm system.

## 2. Data and Methodology

Space-based lightning imagers are staring instruments that continuously monitor the 777.4 nm neutral oxygen emission line triplet for transient optical pulses produced by lightning (NOAA-NASA, 2019). Recording lightning emissions in a narrow band around the neutral oxygen triplet permits lightning imagers to detect total lightning (cloud-to-cloud and cloud-to-ground) with a high detection efficiency during both day and night (Boccippio et al., 2002). These instruments consist of charge-coupled device (CCD) focal plane arrays behind sensor optics that register "events" in pixels that light up above a dynamic threshold that describes the steady-state cloud top radiance in the absence of lightning. Events are the fundamental observations that describe lightning from space. Event data contains information on the location and optical energy of the cloud top pixel illuminated by lightning as well as the precise time of the optical pulse.

The event data provided by LIS and GLM are clustered into features that describe physically complete and distinct lightning flashes. These flashes comprise a standard NASA (LIS)/National Oceanic and Atmospheric Administration (NOAA) (GLM) lightning product that is used to quantify flash rates from individual thunderstorm features (Cecil et al., 2005; Zipser et al., 2006) or average flash rates across the globe (Albrecht et al., 2016; Boccippio, Goodman, et al., 2000; Cecil et al., 2014, 2015). Because family links between parent/child features are preserved in these data sets, the flash cluster data can also be used to document flash characteristics.

When examining the characteristics of individual flashes, it is important to consider how these flash cluster features are constructed and what special circumstances can arise during real-time GLM processing that might result in flashes being artificially modified by the ground system software. Section 2.1 provides a general overview of the core flash clustering algorithm used with both LIS and GLM. Section 2.2 then discusses how the scientific LIS and operational GLM clustering routines differ from this common algorithm, and what coincident meteorological measurements are available for each imager on their respective satellite platforms. Section 2.3 demonstrates artificial GLM flash splitting and describes our methodology for repairing the split flash clusters. Finally, section 2.4 defines distinct flash types that will be evaluated in this study.

### 2.1. Optical Lightning Flash Clustering Algorithm

The event data provided by LIS and GLM are clustered into more complex features that describe lightning for operational and scientific applications. Christian et al. (2000) and Mach et al. (2007) document the lightning flash clustering algorithm developed by NASA for LIS while Goodman et al. (2010) describe the operational Lightning Cluster Filter Algorithm (LCFA) used with GLM. The following discussion summarizes

these two Algorithm Theoretical Basis Documents to detail the commonalities between these two algorithms.

Events in the same 2-ms frame are first clustered into "groups" that represent distinct cloud regions that are simultaneously illuminated by lightning. Events that occur in neighboring pixels that share a border or corner with one another are considered to be part of the same group. Though these group features are meant to describe distinct optical pulses produced by lightning, they do not correlate one to one with the occurrence of physical processes such as strokes. The 500 Frames Per Second (FPS) frame rate of the NASA heritage imagers balanced engineering limitations with measurements of the durations of optical lightning pulses recorded from above the cloud top (Mach et al., 2007). High-altitude aircraft measurements place the median pulse width at ~0.4 ms (Christian et al., 1989; Christian & Goodman, 1987; Goodman et al., 1989; Mach et al., 2005). Thus, a single 2-ms group feature may contain multiple optical pulses. On the other hand, some lightning phenomena can generate optical emissions that persist over multiple frames. Examples include continuing currents (Bitzer, 2017), gigantic jets (Boggs et al., 2019), and K process waves in horizontally expansive lightning channels (Winn et al., 2011).

The LIS and GLM flash clustering algorithms define lightning flashes as collections of groups that are near in space and time. They use three terms in georeferenced coordinates to determine whether two or more groups should belong to the same flash: the east-west distance (dX), the north-south distance (dY), and the time difference (dT). These displacements are compared with specified threshold values that define the maximum distance ($A_{xy}$) and the maximum time ($A_t$) between groups in the same flash. The space thresholds vary between the lightning imagers according to their pixel sizes.

Two different mathematical models have been used to produce lightning cluster features: one based on a box distance function, and another based on a weighted Euclidian distance (WED) function. In the box distance approach, any radiance-weighted group centroid that is within the specified distance and time thresholds of another group centroid will be assigned to the same flash. Given that "true" evaluates to a numerical value of 1, two groups will be clustered into the same flash if BOX = 3 in the following equation:

$$BOX = \left[|dX|<A_{xy}\right] + \left[|dY|<A_{xy}\right] + \left[|dT|<A_t\right] \tag{1}$$

In the WED approach, however, the clustering function is defined as follows:

$$WED^2 = \left(\frac{dX}{A_{xy}}\right)^2 + \left(\frac{dY}{A_{xy}}\right)^2 + \left(\frac{dT}{A_t}\right)^2 \tag{2}$$

and groups with a WED value less than 1 will be clustered into the same flash.

Both LIS and GLM use the WED model to produce physically distinct lightning flash features. Only the previous Optical Transient Detector (OTD; Christian et al., 2003) used the box distance approach to construct flashes. However, LIS uses the box distance approach to cluster lightning flashes into an area of interest (or "area") features that approximate thunderstorm snapshots. Groups data are replaced with flash-level data, and then (1) can be applied without a temporal term and with $A_{xy}$ = 16.5 km to define unique area features. The temporal term is neglected because areas are only produced routinely for instruments in low Earth orbit that have a limited view time over each thunderstorm on the order of 1–2 min. The temporal term would be necessary for platforms in geostationary orbit such as GLM to prevent overgrouping.

Because the LIS and GLM flash clustering algorithms do not include a feature that accounts for long-lasting optical signals, Peterson, Rudlosky, et al. (2017) defined an intermediate "series" feature to cluster multiple groups within the same flash that describe sustained periods of optical emission. Series features are comprised of all groups in a flash that occur within a specified number of frames of one another. The exact number of allowed empty frames depends on the intended application for the series data. Peterson, Rudlosky, et al. (2017) produced series cluster data sets with 0, 1, and 2 empty frames allowed between groups in the same series. A 1-frame gap is considered to be the "default" case because it resolved an issue where flashes with extensive lateral development frequently had series split by single empty frames when the light curves (usually near the threshold for detection anyways) momentarily dropped below the minimum detection threshold. Allowing a 1-frame gap prevents this splitting while still clustering isolated lightning pulses as separate series features.

Series may be labeled as "bright series" if they contain particularly radiant groups relative to the other groups in the flash. We make this distinction by computing the mean and standard deviation for the energies of the groups in each flash. Because flashes are dominated by dim optical pulses (i.e., cloud pulses) with only a few bright groups (i.e., strokes and K changes), we select any group that exceeds one standard deviation above the mean (1σ) as a "bright group." Any series that contains a bright group is designated a "bright series."

## 2.2. Differences in Clustering and Coincident Observations Between LIS and GLM

### 2.2.1. The LIS

There have been two deployments of LIS in low Earth orbit. The first LIS deployment was on the TRMM satellite (Blakeslee, 1998) whose sensor package also included a Microwave Imager (TMI), Precipitation Radar (PR), and Visible and Infrared Scanner (VIRS) (Kummerow et al., 1998). The wealth of coincident measurements made TRMM an ideal platform for investigating the microphysical origins of atmospheric electrical phenomena.

The TRMM satellite operated for 17 years between November 1997 and April 2015. It had an initial orbital altitude of 350 km that was boosted to 402 km in August 2001, and an orbital inclination of 35°. Coincident observations between the LIS, TMI, VIRS, and PR are limited by the relatively narrow 215 km swath width of the PR but are available throughout the tropics up to 36° latitude. The lower altitude of TRMM allowed the LIS instrument to have a smaller pixel size than OTD or GLM and thus resolve cloud regions illuminated by lightning in finer detail. TRMM-LIS pixels were 4–5 km across and of comparable scale to TRMM-PR and TRMM-VIRS pixels (Kummerow et al., 1998).

We previously collocated LIS pixels that registered events with their corresponding PR, TMI, and VIRS pixels to produce "illuminated cloud features" (ICFs; Peterson, Deierling, et al., 2017) that describe the cloud region bounded by the footprint of every LIS flash that occurred within the PR swath. In this study, we extend the ICF concept to thunderstorm scales and construct new "illuminated storm features" (ISFs) that capture contiguous raining regions (radar precipitation features—RPFs; Liu et al., 2008) that are also illuminated by lightning. ISFs differ from ICFs in that they may be illuminated by multiple flashes, and nonraining cloud regions illuminated by lightning will not be counted as part of this new ISF feature.

TRMM ICFs and ISFs provide a means for quantifying the sizes of lightning-producing storm regions and identifying whether they are convective, stratiform, or anvil clouds. As in previous studies (i.e., Peterson & Liu, 2011, 2013) we define "convective" regions as having a nonzero near-surface PR rain rate and a "convective" rain type reported by the TRMM 2A23 algorithm (Awaka et al., 1998). We similarly define "stratiform" regions as having a nonzero near-surface rain rate and a 2A23 "stratiform" rain type designation. All pixels that lack rainfall near the surface are assumed to be "anvil" clouds.

A second LIS deployment is currently hosted on the International Space Station (ISS) (Blakeslee, 2017; Blakeslee et al., 2014). The ISS has a comparable orbital altitude to the TRMM satellite at 400 km but an increased inclination of 51°. ISS-LIS can thus detect lightning in nearly every region of the globe with notable thunderstorm activity at a similar pixel resolution to TRMM-LIS. While the ISS lacks the meteorological instrumentation that was available on TRMM, ISS-LIS provides temporal overlap with GLM that is useful for cross validation.

The same flash clustering algorithm is employed with both LIS instruments. It uses the WED clustering technique for flashes and the box distance technique for producing areas. The distance threshold for flash clustering ($A_{xy}$) is 5.5 km, while the time threshold ($A_t$) is set to 330 ms. There is a special case in flash clustering where new groups could belong to multiple existing flashes. LIS employs a "first fit" solution to this problem (Mach 2019, personal communication) where new groups are always assigned to the earliest candidate flash. The first fit method is also used to assign a flash to one of multiple possible areas (Mach et al., 2007).

### 2.2.2. The GLM

The GLM is the first lightning imager to be placed into geosynchronous orbit (Rudlosky et al., 2018, 2020). It was included in the sensor package of the GOES-R series of satellites operated by NOAA which will provide observations of lightning across the western hemisphere until at least 2035 (Goodman et al., 2013).

Two GOES-R series satellites are currently in orbit. GOES-R was launched in November 2016 and became GOES-16 in the GOES East position at 75.2°W after calibration and validation (Rudlosky et al., 2018). GOES-S (now GOES-17) followed in March 2018 to take the GOES West position at 137.2°W. The two

platforms provide continuous coverage of the lightning threat across the Pacific and Americas chimney regions of the Global Electric Circuit from 54°N to 54°S. The two GLM sensors view lightning from an orbital altitude of nearly 36,000 km above the Earth compared to the few hundred kilometer altitudes of previous instruments. Despite this significantly higher vantage point, improved optics allow GLM to image its hemispheric-scale domain with a relatively uniform 8–9 km pixel size that increases to 14 km at the edge of its field of view (FOV) (Goodman et al., 2013).

The GOES-R series spacecraft also include ABI, NOAA's next generation geostationary multiband imager (Schmit et al., 2017, 2018). ABI scans typically consist of full disk imagery every 10 or 15 min (depending on operating mode), imagery of the continental United States (CONUS) every 5 min, and two commandable mesoscale sector images that each update every minute (mesoscale sector imagery is available every 30 s when the two sectors overlap). The present study analyzes storm evolution in the ABI data by constructing contiguous cold cloud (<235 K) features from the Channel 14 longwave infrared (11.2 μm) brightness temperatures. The 235 K threshold is sufficient to distinguish between individual storm systems, but will integrate organized mesoscale systems into a single satellite feature.

The GLM flash clustering algorithm (Goodman et al., 2010) is based on the WED approach used with LIS, but with a few notable modifications for operational efficiency to keep up with real time. First, a coherency filter is applied to GLM observations. In order for a flash to be considered valid, two distinct events must be detected. The first of these events will not make it through the LCFA, however, so GLM flashes may miss the initial optical pulse from each flash. Second, the GLM LCFA applies the WED function to constituent event locations in each group. Third, the GLM algorithm uses a "full fit" group assignment scheme where groups that could belong to multiple existing flashes cause the candidate flashes to be merged together into a single flash feature. Fourth, the GLM flash clustering algorithm does not produce an area product. The processing stops at the flash level. For GLM flashes, $\boldsymbol{A_{xy}} = 16.5$ km and $\boldsymbol{A_t} = 330$ ms.

### 2.3. GLM Flash Cluster Splitting and Other Caveats

Unlike the legacy lightning imagers, GLM is an operational instrument that has strict latency requirements. The stream of event detections coming from its hemispheric FOV can easily overwhelm the clustering algorithm in the ground system software. The GLM LCFA ensures efficient clustering within its latency requirements by placing hard thresholds on the maximum number of events per group, groups per flash, and flash duration. Whenever a flash/group exceeds one of these thresholds, the LCFA will terminate the feature and define a new feature with any subsequent events.

Since these thresholds are set relatively low (i.e., a maximum of 101 groups per GLM flash compared to a maximum of 2,000 groups per LIS flash), large groups and complex flashes observed by GLM will be artificially split into multiple clusters. The effect of this splitting can be observed by comparing GLM measurements with ISS-LIS. Figure 1 illustrates a particularly large and complex flash in the ISS-LIS data along with all GLM lightning activity in the same temporal and spatial window.

This 112 group ISS-LIS flash with a 64 km maximum group separation was observed on 13 July 2018 at 2:47:18 UTC. Three GLM flashes were defined during this window. To determine whether this is a case of artificial splitting, we applied equation (2) to the groups in these three GLM flashes, and found that they should all belong to the same flash cluster. If we correct the LCFA flash splitting, then the combined GLM flash would consist of 303 groups in 1,264 ms spanning a horizontal distance of 100 km. The larger flash footprint and 3 times greater group count in the same time window suggests that GLM can resolve more of the optical signals (i.e., more groups) from the flash than ISS-LIS. This is particularly evident between 400 ms and 750 ms in the flash time series where GLM measures a single long-duration series compared to the multiple 5–10 ms series recorded by ISS-LIS.

Even with their sensitivity and pixel size differences, GLM and ISS-LIS still give the same overall picture of the evolution and lateral structure of this example flash that is not dissimilar to LMA depictions of horizontal lightning channels. They primarily differ on what details each instrument can resolve. What is most important for this work, however, is that both instruments agree on its characterization (see section 2.4). After repairing the GLM clustering, both sensors identify it as a single lightning flash with extensive lateral development.

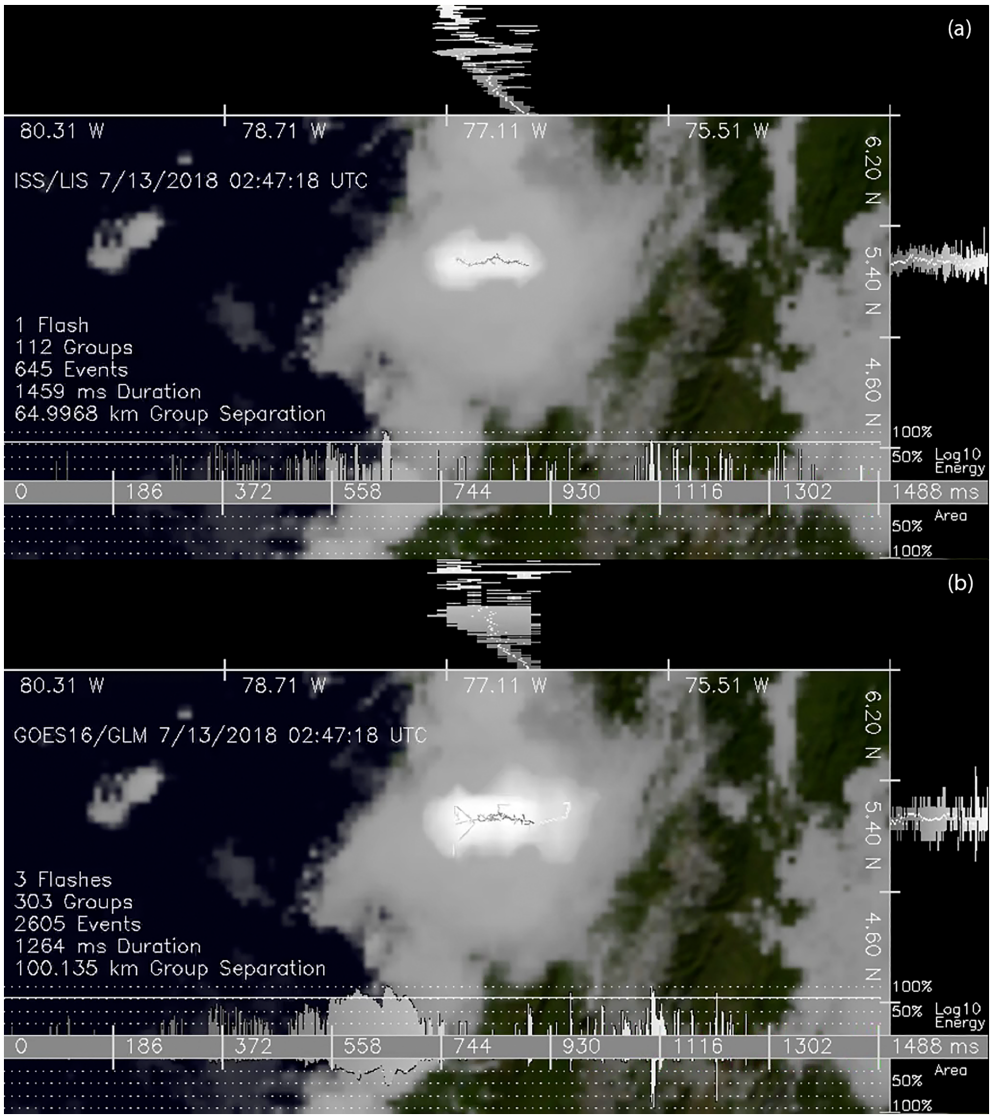


**Figure 1.** The plan view, group extent by longitude and latitude, and time series of group LOG10 (energy) and area for the same propagating flash observed by (a) ISS-LIS and (b) GLM. The energy and area time series are depicted as a percentage of the maximum for the flash. The 1-sigma energy level for the flash is depicted as a solid horizontal line.

We mitigate GLM clustering issues by reprocessing the entire 2018 operational Level-2 flash cluster data produced by the LCFA to identify flashes that should be clustered together according to the WED model described above and then recombine the artificially split clusters (Peterson, 2019a). GLM flashes clustered properly by the LCFA are not modified.

GLM flash splitting is not the only factor that causes LIS and GLM to report different flash rates and flash characteristics over the same window. There are also differences in artifact filtering in the raw event data, differences in background illumination, and curvature effects between LEO and GEO that can alter what each imager records. Because correcting these factors is beyond the scope of the current study, we focus on using LIS measurements to gain insights into GLM trends. We do not perform a full cross validation of the two instruments. The presented results are thus most applicable near the center of the GLM FOV, which provides the closest geometric comparison between LIS and GLM observations. It should be understood that additional refinements are required near the edge of the GLM FOV where storms are being observed from the side rather than from directly above.

Moreover, lightning is not the only transient optical phenomenon that is detected by GLM. With its GEO orbit and staring hemispheric coverage, GLM is subject to a considerable amount of solar contamination through glint (reflections off water and cloud surfaces) and solar intrusion directly into the instrument optics. GLM has also been shown to detect bolides breaking up in the Earth's atmosphere (Rumpf et al., 2019). Because these nonlightning processes will generate false alarms in our analyses (particularly glint), we carefully choose a GLM domain that is free of such artifacts. For reference, supporting information Movie S1 shows a broader CONUS domain for the time period of interest that includes regions where solar contamination is evident.

### 2.4. Definitions of LIS and GLM Flash Types

This study examines how frequently thunderstorms produce four types of lightning according to their optical appearance: elongated flashes, large stationary flashes, propagating flashes, and superbolt flashes. Large stationary flashes and propagating flashes are, in most cases, subtypes of the elongated optical flash category. Elongated flashes are defined in Peterson, Deierling, et al. (2017) as flashes whose maximum separation of events exceeds 2 times the characteristic radius of the flash (i.e., the characteristic diameter). Characteristic radius ($r_c$), is defined from the reported illuminated footprint area ($A_f$) of the flash as follows:

$$r_c = \sqrt{\frac{A_f}{\pi}} \tag{3}$$

Conceptually, the characteristic radius describes the size of a perfectly circular flash with the same footprint area—for example, if the flash were a point source of optical radiance embedded in a homogeneous and infinite planar cloud (Light, Suszcynsky, Kirkland, et al., 2001; Peterson, 2014).

Large stationary flashes illuminate an expansive cloud top footprint, but do not change position on the CCD array between groups. Since group locations are calculated as a radiance-weighted centroid, group displacements can represent fractions of a pixel. We define large stationary flashes as those whose maximum group separations are less than the diameter of 1 pixel with flash footprint areas exceeding 800 km$^2$. Propagating flashes (e.g., Figure 1) are defined as having groups whose centroids are separated by their characteristic radius. These thresholds are arbitrary, but consistent with Peterson, Deierling, et al. (2017) and capture the top 5–10% of LIS and GLM flashes in both land and ocean regions.

The fourth and final flash type is the LIS/GLM superbolt. The term "superbolt" is given to some of the most energetic optical emissions from lightning (Turman, 1977). We define superbolts in the LIS and GLM data sets as having a maximum group radiance at least 100 times greater than the average group radiance for the imager in question.

## 3. Results

The coincident space-based lightning and thunderstorm measurements described in section 2 are used to examine how optical flash characteristics vary with the scale and organization of the parent thunderstorm. Section 3.1 uses TRMM statistics to examine which types of clouds tend to produce each of our flash types from section 2.4 and how the flash type frequencies change with PR metrics for thunderstorm scale and organization. Section 3.2 then uses continuous GOES-16 measurements to examine the joint evolution of GLM flash characteristics and ABI thunderstorm feature properties.

### 3.1. Statistical TRMM Relationships Between Flash Characteristics and Thunderstorm Scale and Organization

#### 3.1.1. LIS Flashes in Convective, Stratiform, and Anvil Clouds

ICFs are first used to quantify how often our four flash types occur in convective, stratiform, and anvil clouds. Results from Peterson, Deierling, et al. (2017), Peterson, Rudlosky, et al. (2017) suggested that large stationary flashes were often reflection cases near the anvil boundaries and that propagating flashes developed from the convective line into the stratiform region, but that study did not quantify how often these flash types occurred in each storm region.

To do this, two-dimensional histograms are constructed based on the ICF area fractions of each PR-based rain type from 16 years of TRMM observations. We calculate these area fractions for each LIS flash by

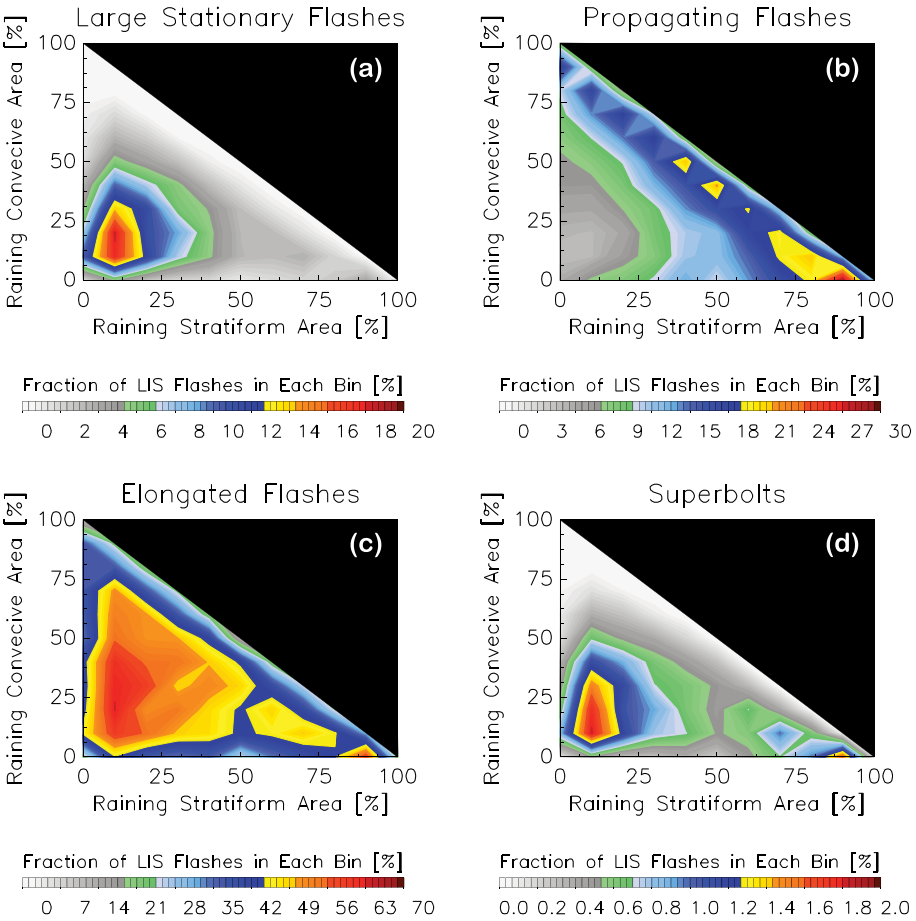


**Figure 2.** Fractions of LIS flashes that are large stationary (a), propagating (b), elongated (c), and superbolt (d) cases according to the area fractions of raining convective and raining stratiform cloud they illuminate.

integrating the total area of collocated PR pixels that match LIS events and then dividing by the total footprint of all matching PR pixels in the flash. These histograms show how often convective clouds (top left of the distributions in Figures 2a–2d), anvil clouds (bottom left) and stratiform clouds (bottom right) produce large stationary flashes (Figure 2a), propagating flashes (Figure 2b), elongated flashes (Figure 2c), and superbolts (Figure 2d). As the previous cases suggest, large stationary flashes are most common in anvil cloud regions (defined as <25% raining convective area and <25% raining stratiform area), where they account for up to 20% of all flashes (Figure 2a). By comparison, large stationary flashes account for <3% of all lightning in convective and stratiform clouds (defined as exceeding a 75% area of each cloud type).

Propagating flashes (Figure 2b) are least common in these anvil/boundary cloud regions. Rather, they are most prevalent along the right-hand diagonal boundary of the histogram, denoting where the convective and stratiform rain types combine to account for nearly 100% of the flash footprint area. The distribution peaks where stratiform clouds make up >90% of the ICF area. In these primarily stratiform clouds, 30% of all lightning falls into the propagating flash category. This supports previous examples of propagating LIS flashes primarily illuminating stratiform regions (see Peterson, Deierling, et al. (2017), Peterson, Rudlosky, et al. (2017).

The large stationary and propagating flash categories are mutually exclusive—with one prohibiting lateral development and the other requiring it. These categories appear to be associated with specific cloud types, with large stationary flashes associated with cloud boundaries and reflections (Peterson, Deierling, et al., 2017; Peterson, Rudlosky, et al., 2017), while propagating flashes requiring favorable thunderstorm charge structures for lateral development. Thus, the relative frequency of these flash types may provide insights into the organization and evolution of the thunderstorm as a whole. For example, if 20% of flashes are large

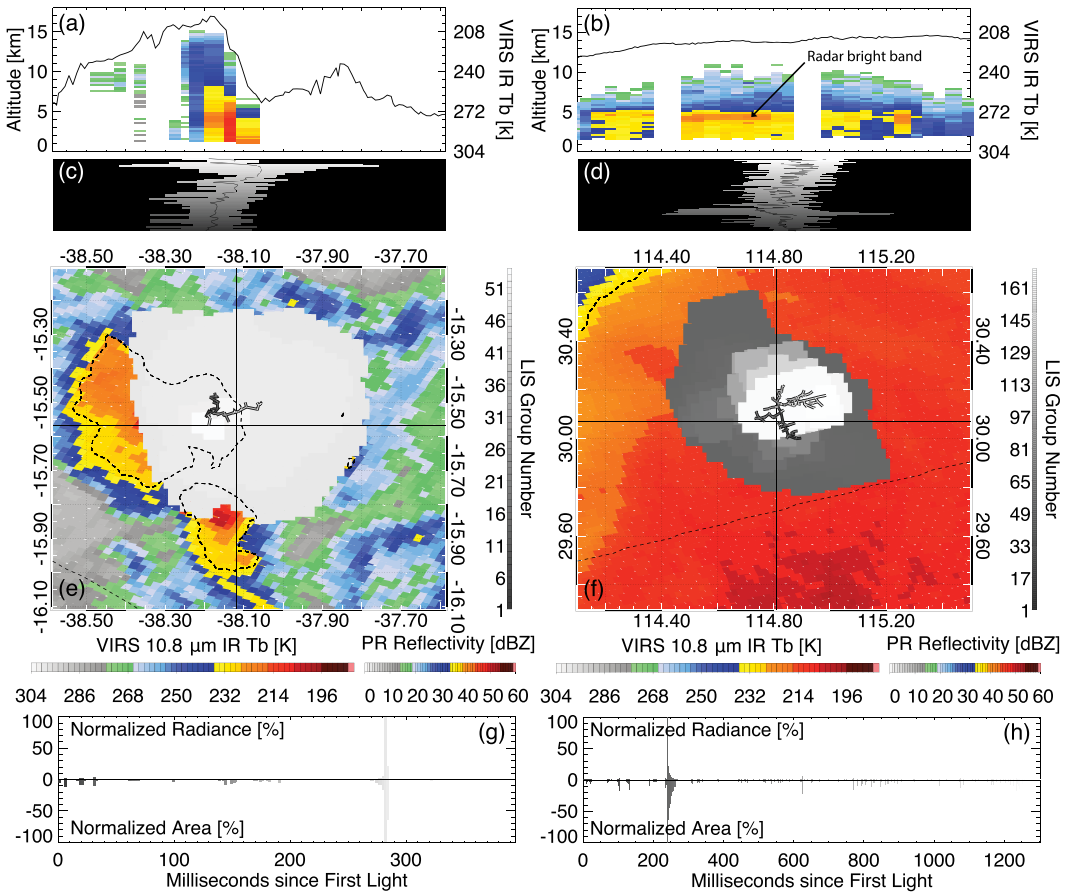


**Figure 3.** Examples of anvil (left) and stratiform (right) superbolts recorded by LIS on the TRMM satellite. (a, b) PR reflectivity and VIRS Channel 4 brightness temperature longitudinal cross sections. (c, d) LIS cross sections showing the longitudinal extent of each group. (e, f) Plan view of VIRS CH4 infrared brightness temperatures (dashed contour bounds 232 K regions) and LIS events (boxes) and groups (lines). (g, h) Time series of normalized LIS group radiance (>0) and group area (<0). All LIS features use the same gray color scale based on time-ordered group number where first light is dark gray and final light is light gray.

stationary and only 1% are propagating, then Figures 2a and 2b suggest that this configuration of large flashes indicates a flashing anvil region. In the opposite case with 20% propagating and only 1% large stationary, then one could infer the presence of a horizontally extensive electrified stratiform region.

This partitioning only works if flash length is approximated by the maximum separation of groups rather than the maximum separation of events. The elongated flash category (Figure 2c) bases its flash length measurement on event separation. Because large flashes tend to take on an elongated appearance regardless of flash structure (Peterson, Deierling, et al., 2017), this distribution convolves the large flashes in Figures 3a and 3b. The distribution peaks at 70% along the nonstratiform axis by capturing ambiguous flashes between the thresholds set by the large stationary and propagating definitions. Generally, the maximum event separation is not considered a good estimate for flash length because (1) reflections off of nearby cloud faces can artificially increase the perceived size of the flash (Peterson, Deierling, et al., 2017; Peterson, Rudlosky, et al., 2017), (2) particularly radiant pulses can cause CCD anomalies (known in the LIS data as "lollypops") that generate nonphysical events that are clustered into the flash (Christian et al., 2000), and (3) it is particularly sensitive to diurnal changes in instrument sensitivity due to varying background illumination (Peterson et al., 2018).

The extreme brightness of lightning "superbolts" leads to some of the largest event separations recorded from space (Peterson, Rudlosky, et al., 2017). Superbolts are particularly radiant pulses that were first identified by the optical payload on the Vela satellites. Superbolts comprise the top <1% of lightning pulse

radiances and are on the order of 100 times more powerful than typical lightning emissions (Turman, 1977). Since these cases result from one particularly radiant pulse on the order of 1 ms, the "length" of the flash based on maximum event separation is entirely dependent on the observation of a single group that lights up thousands of square kilometers of surrounding thundercloud. The maximum group separation, meanwhile, is not drastically increased by these radiant pulses, resulting in up to a 100 km disagreement between flash "lengths" based on the maximum group separation and the maximum event separation (Peterson, Rudlosky, et al., 2017).

Figure 2d examines the types of clouds that contain these superbolt flashes. Unlike the large stationary and propagating flash categories that each had single well-defined peaks, the superbolt distribution has two. LIS superbolts are most common (up to 2% of all flashes) embedded within anvil cloud regions (bottom left) or almost completely contained within raining stratiform clouds (bottom right). This suggest that the term "superbolt" actually describes two scenarios that can give rise to particularly radiant optical lightning pulses.

Anvil superbolts occur near boundaries or breaks in the cloud where no near-surface precipitation is recorded by the TRMM PR. An anvil superbolt example is shown in the left column of Figure 3. In this anvil superbolt case, the center of the flash (where the horizontal and vertical lines intersect) is located near the eastern edge of the 232 K CH4 contour for the parent thunderstorm. The PR and VIRS measurements shown in Figure 3a indicate an overhanging anvil only on the western flank of the thunderstorm. Thus, the optical emissions from the flash that escape the eastern flank have a relatively unimpeded path to reach the satellite. This superbolt is an "anvil" superbolt because the majority of the flash footprint is outside of this convective PR feature. The flash does light up the western anvil of the storm, but it primarily illuminates the tops of lower (warmer) clouds to the east of the parent thunderstorm (CH4 $T_b > 232$ K in Figure 3e). This case shows that direct measurements and reflections can both contribute to the pulses that we deem "superbolts" and favorable viewing conditions (near a boundary, with surrounding clouds) can make even normal lightning appear to be larger and brighter than it otherwise would.

Anvil superbolt cases agree with Kirkland's (1999) observations of the superbolts recorded by the photodiode detector on the FORTE satellite. These FORTE superbolts were of both polarities and included cases that arose from intracloud discharges as well as cloud-to-ground strokes. Kirkland (1999) suggested that the path between the superbolt emitter and the satellite was relatively clear compared to typical lightning due to relatively narrow pulse widths (i.e., less temporal broadening from Mie scattering). Without finding a unique signature in the coincident FORTE RF data, Kirkland (1999) concluded that these superbolts were simply the extreme of the normal lightning distribution.

Stratiform superbolts still may represent a unique set of lightning physics that could warrant a separate designation. In recent years, superbolts have been linked to powerful discharges from intense mesoscale convective systems (MCSs) that may accompany transient luminous events (Blanc et al., 2007). This type of storm also produces the large electrified stratiform regions where we find cases of stratiform superbolts in Figure 2d. The right column of Figure 3 illustrates an example of a stratiform superbolt. As with the previous anvil case, the flash footprint is large but all of the triggered pixels are located in a stratiform region with a radar bright band at ~ 5 km altitude visible in Figure 3b. The stratiform nature of the illuminated cloud prevents a "shortcut" explanation for how the flash can become so bright. Instead, the flash could have been this radiant if it occurred near the cloud top (possibly as an upward discharge) or if it was a positive discharge with a very high peak current (as noted in Turman, 1977 with additional discussion in Uman, 1978). It is also worth noting that stratiform superbolts often have continuous emission for more than 10 frames (20 ms) following the optically bright pulse (Figure 3h) whose incident energy falls over time and may be continuing current (Bitzer, 2017). This can also be seen in the stratiform case from Figure 5 in Peterson, Rudlosky, et al. (2017), but not the anvil case in Figure 3g.

#### 3.1.2. Variations in LIS Lightning Characteristics by Overall Thunderstorm Scale and Mode

This section moves beyond ICFs that describe clouds illuminated by single flashes to ISFs that bound entire storm features illuminated by lightning. Statistics are generated to show how LIS flash characteristics generally vary based the scale and organization (i.e., convective/stratiform partitioning) of the parent thunderstorm (Figure 4). Isolated and new convection will consist of primarily convective features by area (i.e., near a 0% stratiform fraction), while mature and dissipating MCSs may have a nearly 100% stratiform area

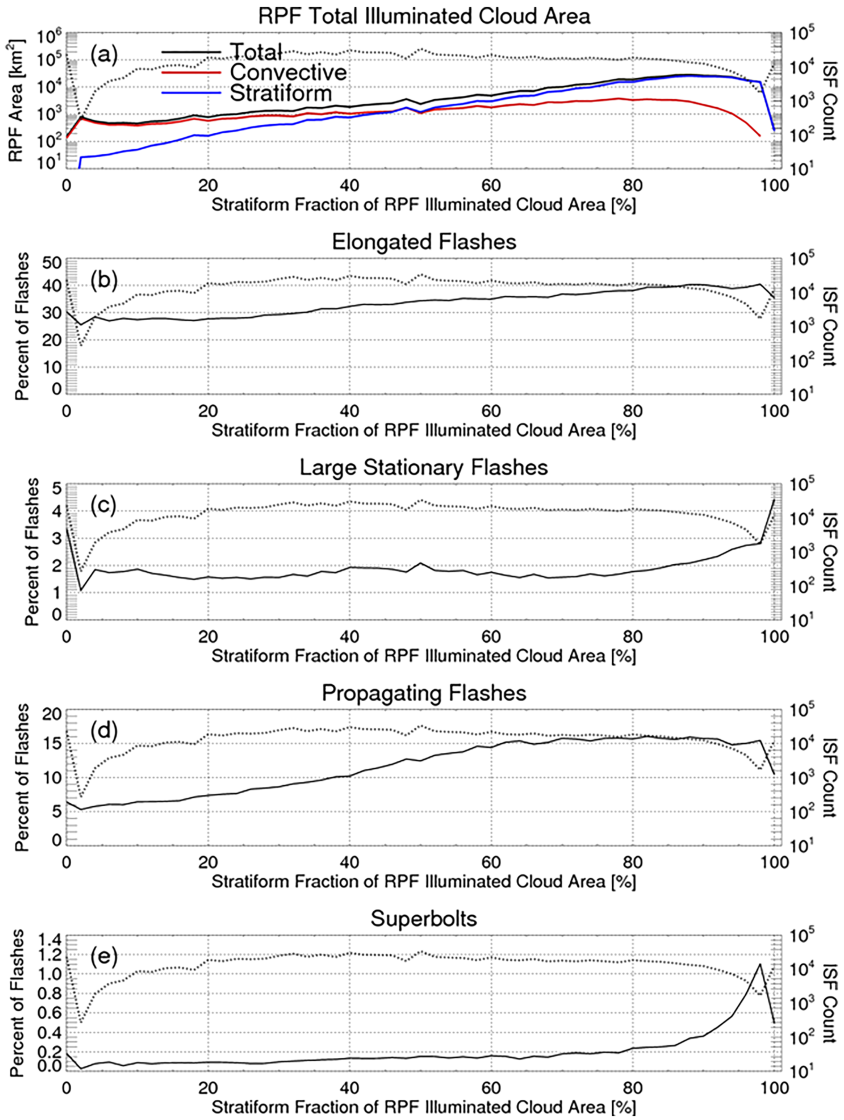


**Figure 4.** Distributions of RPF area (a), elongated flash fraction (b), large stationary flash fraction (c), propagating flash fraction (d), and superbolts fraction (e) by the stratiform area fraction of the RPF region illuminated by the flash. Dotted lines show the sample size per bin (right axis).

fraction. The overall ISF size (or the total RPF area that is illuminated by lightning) is then considered in Figure 5 as a proxy for thunderstorm scale.

Figure 4a shows the average total, convective, and stratiform areas as a function of ISF stratiform area fraction. All three measures of feature area increase as the ISFs becomes more stratiform, with the stratiform area growing most rapidly. This is consistent with the upscale growth and charge advection that typically accompanies thunderstorm maturation. Figures 4b–4e compute the fractions of all flashes that fall into one of the four classifications. Elongated flashes account for nearly 30% of all flashes in entirely convective storms, increasing to over 40% for mostly stratiform storms (Figure 4b). Large stationary flashes occur most often in 0% stratiform ISFs, but are otherwise uncommon in generally convective features (Figure 4c). The frequency of large stationary flashes remains at <2% of all lightning until the stratiform fraction reaches 80%, when the large stationary flash fraction doubles to reach an overall maximum of 4.4% for entirely stratiform features.

Propagating flashes (Figure 4d) account for only 5% of all flashes in entirely convective storms and increase in frequency with stratiform area fraction until the ~65% stratiform mark. More mature storms based on this

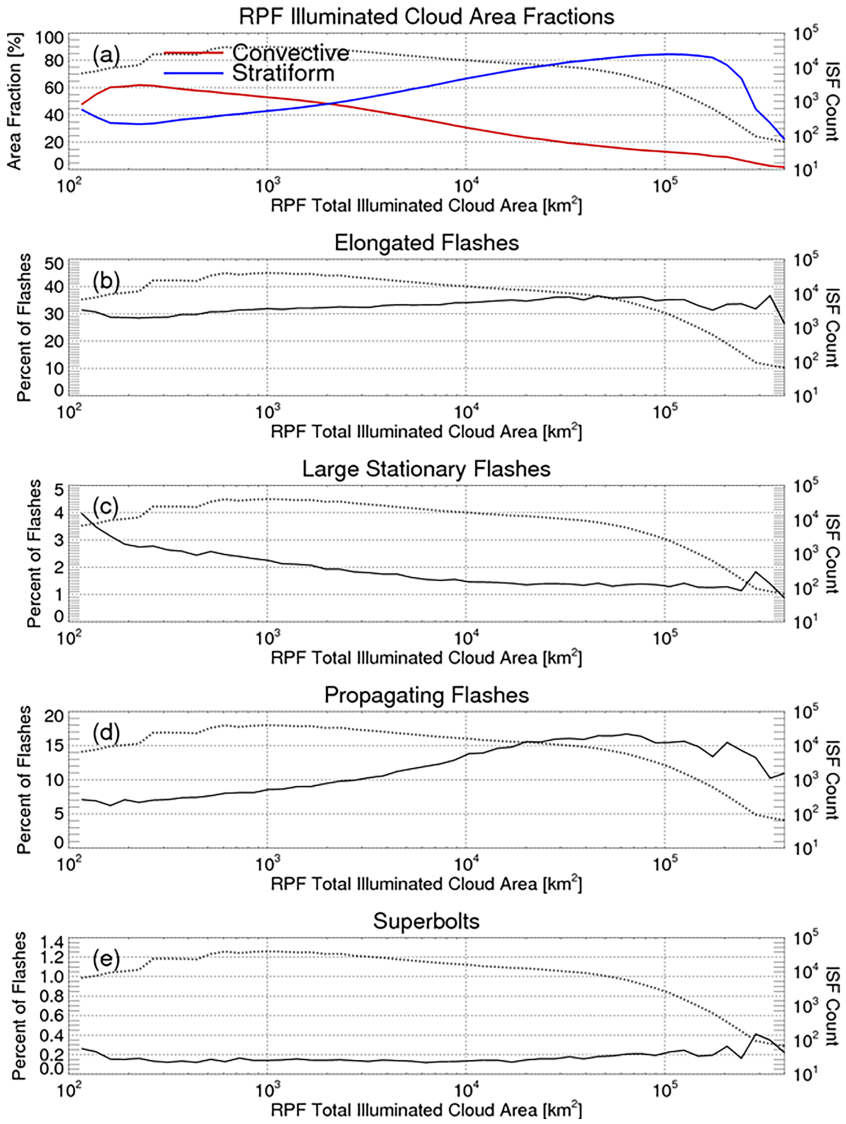


**Figure 5.** The same as Figure 4, but for the total area within the RPF illuminated by the flash.

proxy maintain a constant 15% propagating flash fraction. The final distribution in Figure 4e shows the proportion of superbolts as a function of the ISF stratiform area fraction. Superbolts are uncommon (<0.2% of all flashes), but spike to >1% in storms that are ~95% stratiform, indicative of the stratiform superbolt scenario discussed in the previous section.

Figure 5 examines how the frequency of each lightning flash type varies with ISF area. The smallest ISFs are a few hundred square kilometers and more convective than stratiform, on average (Figure 5a). However, as ISF size increases, the convective area fraction decreases while the stratiform area fraction grows. The elongated flash fraction remains fairly stable at ~30% throughout the range of ISF areas (Figure 5b), but the large stationary flash fractions and propagating flash fractions change considerably with ISF size. The large stationary flash fraction (Figure 5c) decreases monotonically with increasing ISF area from 4% of all flashes at 100 $km^2$ to 1.2% at $10^5$ $km^2$. This steady decline contrasts the spike at 0% stratiform area in Figure 4c and shows that both thunderstorm scale and organization are important factors influencing the frequency of large stationary flashes. The propagating flash fraction, by contrast, mirrors the steady increase in stratiform area from Figure 4d. Finally, the superbolt fraction remains close to 0.2% for ISFs of all sizes. Unlike the stratiform area fraction in Figure 4, the

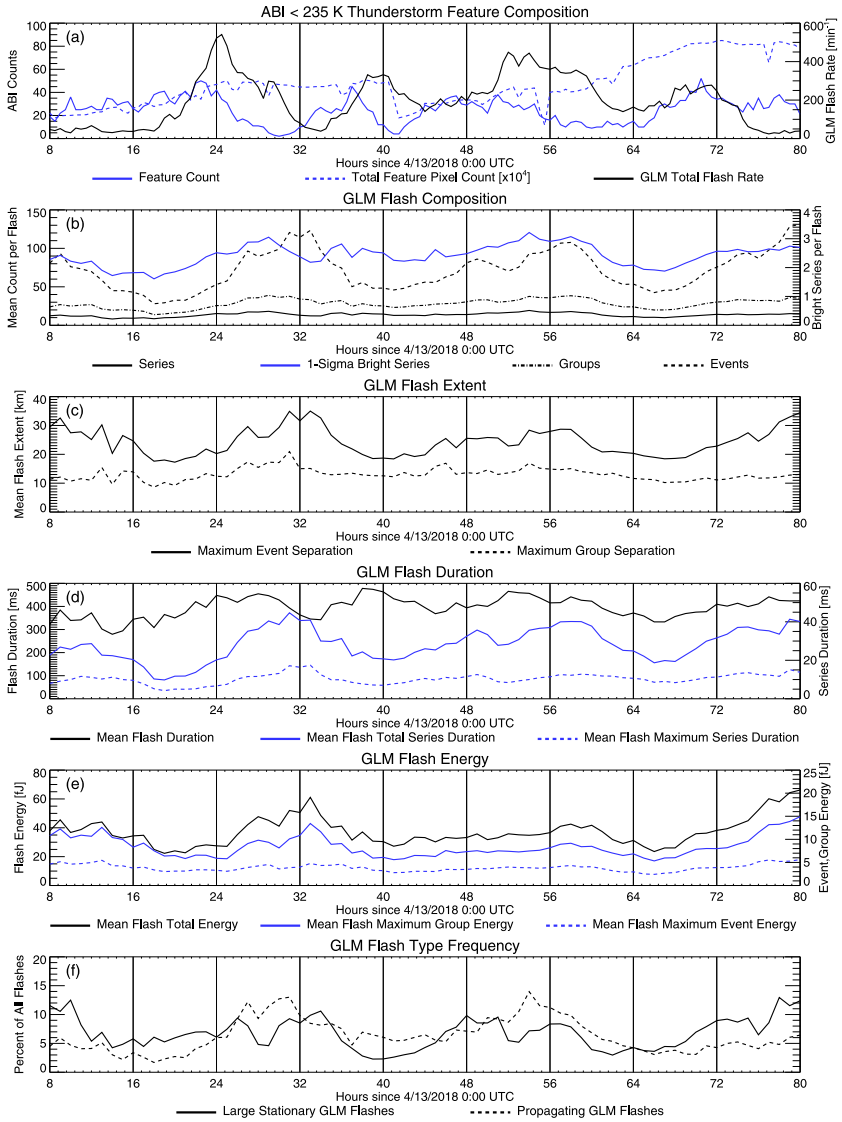


**Figure 6.** Time series of (a) the composition and flash counts of ABI cold cloud thunderstorm features, (b) average GLM flash composition, (c) average flash extent, (d) average flash duration, (e) average flash energy, and (f) frequency of large stationary and propagating GLM flashes.

sample size in Figure 5 decreases substantially with increasing ISF area. Thus, the superbolt fraction increasing to 0.4% near $10^6$ $km^2$ may not be physical.

The distributions in Figures 4 and 5 support the idea that reflections produce large stationary flashes in small isolated convection and dissipating convection, while propagating flashes accompany mature convection.

### 3.2. GLM Observations of Changing Flash Characteristics From a Single Long-Lived Storm

The previous section took a statistical approach with LEO snapshots to show how flash characteristics vary in response to the related precipitation and electrical structures of thunderstorms. However, GLM's staring hemispheric coverage permits examination of lightning flash characteristics as individual storm systems evolve. In this section, we look for evidence of these trends in a single long-lived MCS that crossed the CONUS over multiple days from 13 April 2018 to 17 April 2018. We expect to find relatively high fractions of large stationary flashes and few propagating flashes accompanying small isolated convection (for example, in the initial stages of the thunderstorm), frequent propagating flashes with few large stationary flashes

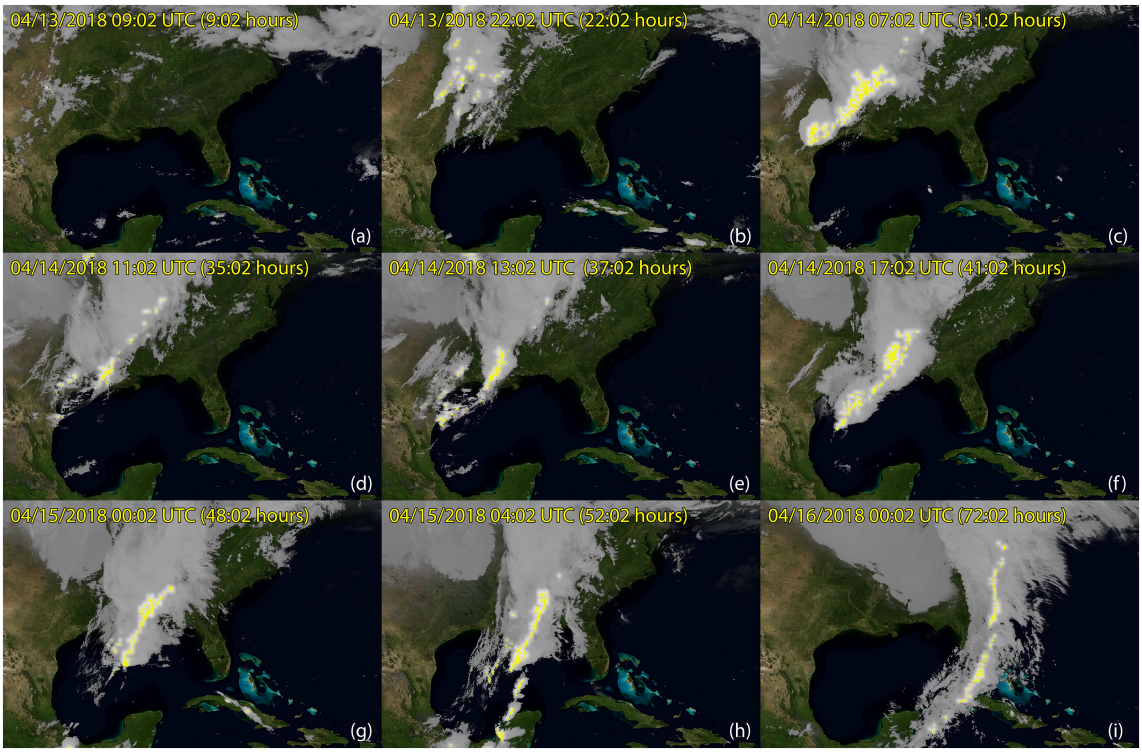


**Figure 7.** Snapshots of ABI and GLM imagery at (a) 09:02 UTC on 13 April 2018, (b) 22:02 UTC on 13 April 2018, (c) 07:02 UTC on 14 April 2018, (d) 11:02 UTC on 14 April 2018, (e) 13:02 UTC on 14 April 2018, (f) 17:02 UTC on 14 April 2018, (g) 00:02 UTC on 15 April 2018, (h) 04:02 UTC on 15 April 2018, and (i) 00:02 UTC on 16 April 2018. The number of hours since 13 April 2018 0:00 UTC are also specified for comparison with Figure 5.

following upscale growth and thunderstorm maturation, and then the return of large stationary flash activity as the thunderstorm begins to dissipate.

Figures 6 and 7 depict the evolutions of ABI contiguous cold cloud thunderstorm features and GLM flash characteristics along the frontal system. Figure 6 shows time series of ABI and GLM measurements, while Figure 7 depicts key points in the storm development as snapshots of ABI/GLM imagery. The GLM flash activity in Figure 7 is integrated over 5-min windows to mirror the cadence of ABI CONUS sector imagery. This imagery is also animated over the entire time period of interest in Movie S1.

Figure 6a traces the number of ABI thunderstorm features, the total feature area (expressed as an ABI pixel count), and the total GLM flash rate for the spatial domain covered by the storm while it was over CONUS or just offshore (18°N, 110°W to 42°N, 75°W). Feature tracking is unnecessary because the frontal system of interest is the dominant source of lightning in this region throughout the period of interest.

The first flashes along the cold front occurred in the 08:00 UTC hour on 13 April 2018. Figure 7a shows the cold cloud features at this time (also Hour 8 in Figure 6). The isolated features over Texas and Oklahoma began to grow and consolidate as new convection initiated along the front. This caused both the ABI total feature area and ABI feature count in Figure 6a to increase over the first 10 hr of thunderstorm activity (Hours 8–18). The first flashes in this initial period contained more series, groups, and events than the flashes that occurred later. In fact, all measures of flash extent and complexity except flash duration decreased with time to reach a local minimum in Hour 18—including the maximum distance separations of groups and events (shown for comparison) (Figure 6c), series duration (Figure 6d), and flash and peak group energies (Figure 6e)

It is important to note that the decline in flash size and complexity precedes the drastic increase in flash rate that began in Hour 18. The opposition between flash rate and flash size discussed in Bruning and MacGorman (2013) does not appear to be the driving force behind this change, as flash rates remain stable over this period. Instead, they seem to be caused by a change in the cloud illumination. During the first 10 hr

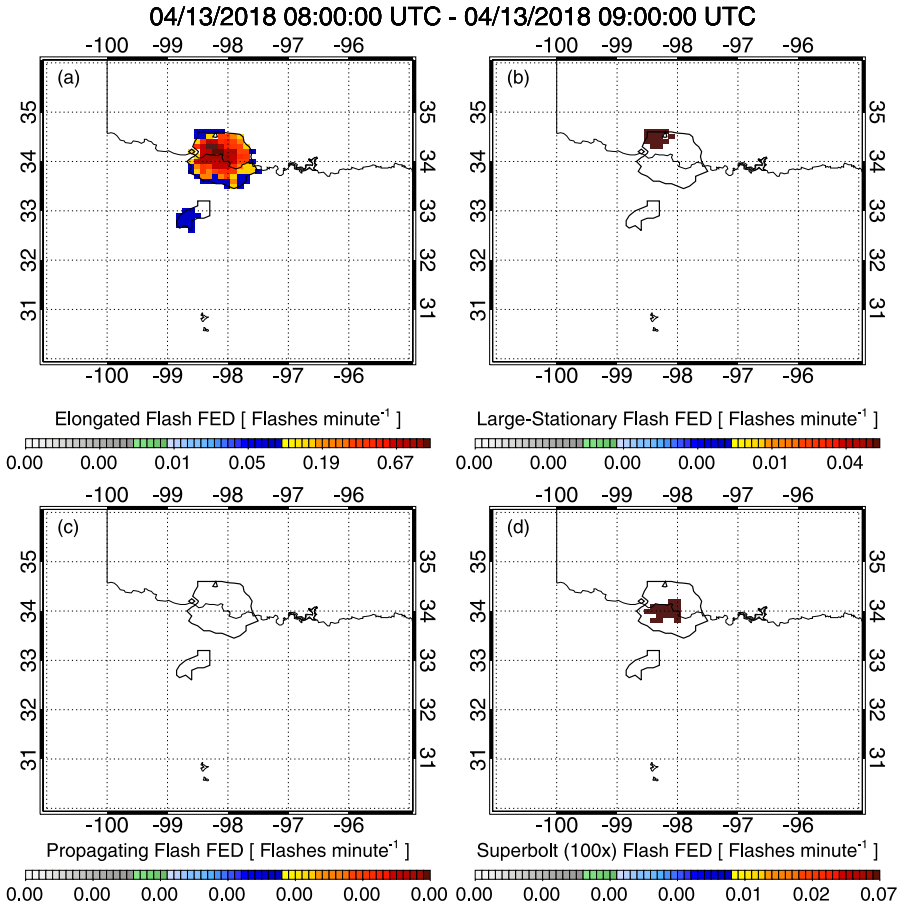


**Figure 8.** GLM 1-hr integrations of the flash Extent Densities (FEDs) for (a) elongated flashes, (b) large stationary flashes, (c) propagating flashes, and (d) superbolts. Solid black contours bound regions with lightning activity. Valid for 08:00 UTC on 13 April 2018 when the storm consisted of disorganized convection.

of Figure 6b, the average number of events per flash dropped from 92 to 28, which was a faster decline than the number of groups per flash that only fell by 10. This means that the optical pulses detected by GLM at Hour 8 were larger with more events per group than those observed at Hour 18. The maximum group energy and maximum event energy curves in Figure 6e further suggest that this is due to brighter overall flashes at the beginning of this period—possibly even our large stationary flashes.

To check whether frequent large stationary flash activity is contributing to this trend, we compute the fractions of all flashes recorded by GLM during each hour that are large stationary flashes or propagating flashes in Figure 6f. Indeed, there is a peak in the large stationary flash fraction during the first 3 hr of this period (Hours 8–11) where more than 10% of all lightning recorded by GLM fell into the large stationary flash category (though not all times had a high number of flashes). Large stationary flashes were twice as common during these first 3 hr compared to subsequent periods, and large stationary flash fractions exceeded the propagating flash fraction (which remained below 6% until Hour 24).

To identify where these large stationary flashes are occurring, Figure 8 focuses on the developing thunderstorms along the Texas-Oklahoma border and plots 1-hr snapshots of flash extent density (FED) between 08:00 UTC and 09:00 UTC on 13 April 2018 for each flash type. Solid lines contour contiguous regions that were illuminated by lightning. This hour-long window captures all initial lightning activity from the cells shown in the figure. Elongated flashes (Figure 8a) were the most common of our four flash types, and were ubiquitous across footprint of the larger northern cell. The first large stationary flash (Figure 8b) occurred during this period and was located along the northern flank of the larger northern thunderstorm feature. This single flash illuminated ~20% of the storm area. No propagating flashes (Figure 8c) were observed,

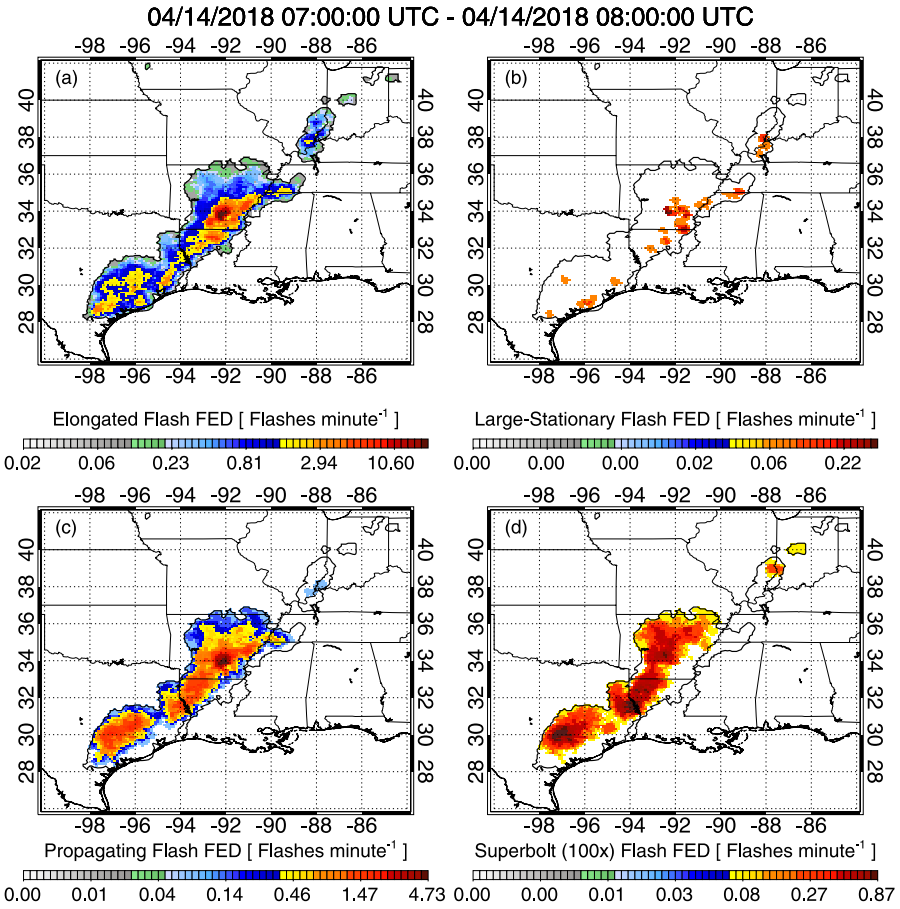


**Figure 9.** As in Figure 8, but valid for 07:00 UTC on 14 April 2018 when the MCS had matured.

but the northern storm did produce two superbolts (Figure 8d) based on our 100 times typical group radiance definition.

The next three hours (Hours 11–14) saw a sharp decline in the large stationary flash fraction. ABI feature counts and total ABI feature area increased until Hours 22–24 (Figure 7b) due to the growth of existing features and the initiation of new convection behind the initial line. Though only half as frequent as in the initial burst, large stationary flashes were still dominant over propagating flashes throughout this period. The propagating flash fraction caught up with the large stationary flash fraction during Hour 24 (00:00 UTC on 14 April 2018). The transition to a propagating flash dominance suggests that the storm was beginning to mature and develop an electrified stratiform region. By this point, the second line of convection had overtaken the first line to form a single MCS (see also Movie S1). This period where the large stationary and propagating flash rates were nearly equal (Hours 24–27) saw the overall GLM flash rate reach its peak and then begin to decline, while the ABI cold cloud area reached its maximum extent (at least while the storm was primarily over land) and began to organize into an increasingly smaller numbers of distinct ABI features (Figure 6a). By Hour 30, this large area of cold cloud contained just two separate ABI features.

The reduction in the ABI feature count coincided with an increase in the number of groups, events, series, and bright series (defined earlier as distinct periods of continuous optical emission that contain a particularly luminous group) (Peterson & Rudlosky, 2019) per flash (Figure 6b), in both the maximum separations of events and groups (Figure 6c), in flash and series durations (Figure 6c), and in flash and group energy (Figure 6d). It is during this period that the first extraordinary cases of propagating flashes can be noted in Figure 7c and in Movie S1. Though these graphics integrate all lightning activity (making individual flashes difficult to discern in high flash rate storm regions), large clusters of lightning extending back behind the

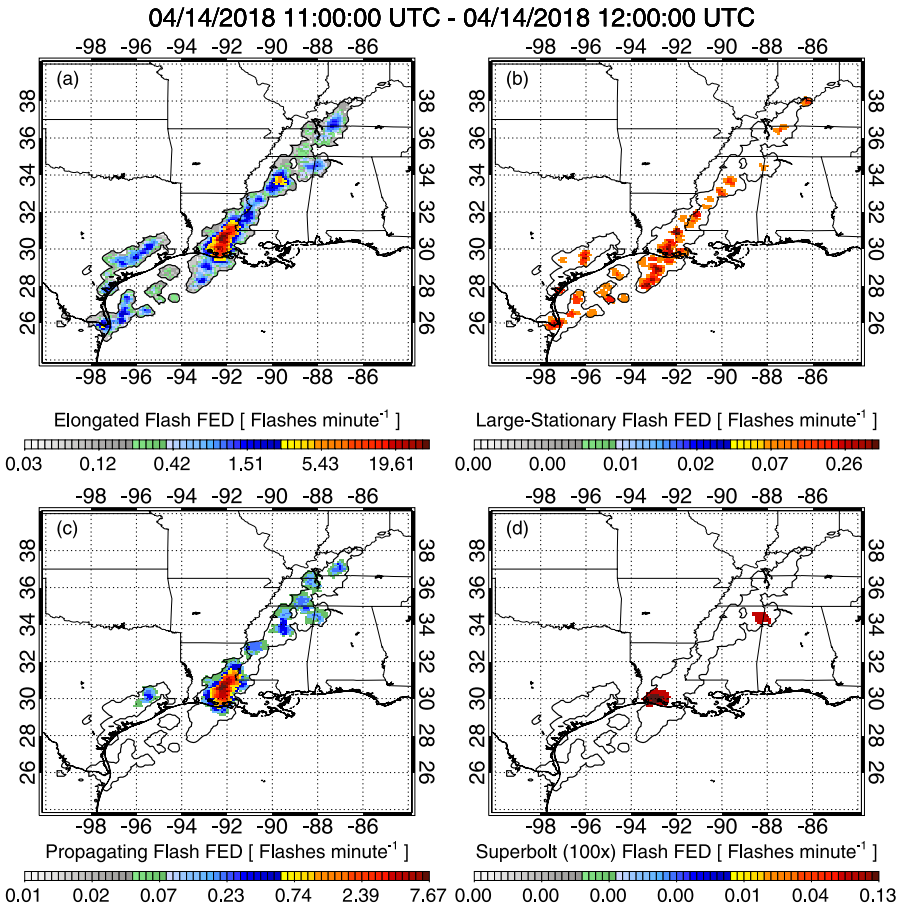


**Figure 10.** As in Figure 8, but valid for 11:00 UTC on 14 April 2018 when the MCS was dissipating.

convective line can be noted in the imagery. Propagating flashes accounted for 2–6% of all lightning in the early stages of the frontal system, but increased to 13% of all flashes by Hour 31 (Figures 6f and 7c).

FED snapshots for Hour 31 (07:00 UTC on 14 April 2018) are shown in Figure 9. While elongated flashes (Figure 9a) could be noted along the front, mostly concentrated in the convective line, large stationary flashes (Figure 9b) were primarily located in the leading anvil to the southeast of convection. Propagating flashes (Figure 9c), meanwhile, extended rearward from the convective line into the trailing stratiform region. Superbolts (Figure 9d) were most common in the trailing stratiform region, but a few anvil superbolts can be noted in the two northeastern GLM features over Illinois and Indiana.

The 6-hr period between 05:00 UTC and 11:00 UTC on 14 April (Hours 29–35) saw a rapid decrease in flash rate followed by an increase in feature count, though the total feature area remained relatively constant (Figure 6a). This was caused by new development along the southern flank of the system becoming disconnected from the primary ABI cold cloud feature while the MCS began to weaken (Figures 6d and 6e). The number of series, groups, and bright series per flash declined during this time of transition, even as the number of events per flash reached a maximum (Figure 6b). Some of the largest flashes by illuminated cloud footprint (Figure 6c) were found during this period, which also had the longest series durations (Figure 6d) and flash and group energies (Figure 6e). There was additionally a brief changeover in Figure 6f from a propagating flash dominance to a large stationary flash dominance, consistent with our expectations for both this new convection and the old dissipating convection.

Figure 10 shows GLM FED snapshots for 11:00 UTC on 14 April 2018 (Hour 35). Lightning had ceased in many portions of the stratiform region by this point in time, causing the front-to-rear width of the primary GLM thunderstorm feature to decrease compared to Figure 9. Large stationary flashes (Figure 10b) occurred throughout the storm, while pockets of propagating flashes (Figure 10c) persisted near the strongest

convection (over Louisiana) and in the northern regions of the storm. Two storm regions produced superbolts (Figure 10d) during this period, and both were located along the flanks of the primary thunderstorm feature.

Over the first day of the storm, its flash characteristics had an initial large stationary flash dominance followed by a propagating flash dominance upon maturation, and then a second large stationary dominance later on. The ABI cold cloud feature properties are consistent with the underlying reasons why we expect such a change to occur (scattering/reflections and stratiform charge structures). Sunrise on the second day occurred in Hour 35 of Figure 6, and flash rates subsequently started to increase along the front. By Hour 41 (17:00 UTC on 14 April), the convective portion of the system had reorganized into a single ABI cold cloud feature (Figure 7f) with thunderstorm activity straddling the Gulf coast. Mean GLM flash counts and maximum event separations decreased by nearly half during this reorganization. Mean series durations and flash and group energies also decreased as propagating flashes once again became the prevailing mode.

Between Hour 41 (Figure 7f) and 48 (Figure 7g), the lightning-producing portions of the storm system moved largely offshore. Thunderstorms developed from the southern flank of the MCS to the Yucatan Peninsula in Mexico (Figure 7h) and merged with the primary feature by Hour 72. This consolidation led to the highest total ABI cold cloud feature area in Figure 6a despite the total flash rate decreasing to less than 50 flashes per minute across the system. The number of events per flash (Figure 6b) increased from 40 in Hour 67 to a high of 130 events per flash at Hour 80 when the entire system began to dissipate. The number of series, bright series, and groups per flash also increased, as did the maximum separation of events, series durations, and the average flash and group energy. While the system moved toward dissipation, the proportion of large stationary flashes increased to its overall maximum of 13% of all lightning while the propagating fraction remained at 5% of all flashes.

## 4. Conclusions

This study uses observations from two different space-based lightning imagers to investigate how the characteristics of lightning flashes viewed from orbit change according to the organization and structure of the parent thunderstorm with an emphasis placed on MCSs. Coincident LIS and PR measurements taken by the TRMM satellite were used to construct statistical relationships between flash characteristics and the types of clouds illuminated by lightning. An anomalously large 20% of flashes in nonraining clouds are of the large stationary variety. These flashes are common near the edges of convective cloud features, as optical energy can escape the side of the cloud to illuminate the faces of neighboring clouds, causing the flash footprint to grow. Propagating flashes that indicate local horizontally stratified charge structures most frequently illuminate stratiform clouds (30% of all lightning). Particularly bright "superbolt" flashes occur primarily in two distinct cloud types. Anvil superbolts are similar to large stationary flashes where optical emissions have a clearer path to the satellite and thus appear brighter than emissions scattered through thick cloud layers. The second type of superbolt occurs embedded almost entirely within regions of stratiform rain regions.

GOES-16 satellite data were used to examine the evolution of a long-lived MCS observed by GLM and ABI over multiple days. The lightning produced by this storm system supported the TRMM-LIS trends based on thunderstorm organization and scale. Early lightning was likely to be large stationary, but the fraction of these flashes declined as the system organized and grew upscale. Propagating flashes became common after the storm reached maturity and developed an expansive electrified stratiform region. Finally, large stationary flashes returned during periods where the system was dissipating.

**Acknowledgments**
This study was supported by NASA Grant NNX17AH63G. The LIS science data set is available online from the NASA Global Hydrology Resource Center DAAC, Huntsville, Alabama, USA. The GLM LCFA and ABI data sets may be obtained from NOAA via their CLASS service. The contents of this paper are solely the opinions of the authors and do not constitute a statement of policy, decision, or position on behalf of NOAA or the U.S. government.

## References

Albrecht, R. I., Goodman, S. J., Buechler, D. E., Blakeslee, R. J., & Christian, H. J. (2016). Where are the lightning hotspots on Earth? *Bulletin of the American Meteorological Society*, *97*(11), 2051–2068. https://doi.org/10.1175/BAMS-D-14-00193.1

Awaka, J., Iguchi, T., & Okamoto, K. (1998). Rain type classification algorithm. *Measuring Precipitation from Space*, *3*, 213–224.

Bitzer, P. M. (2017). Global distribution and properties of continuing current in lightning. *Journal of Geophysical Research: Atmospheres*, *122*, 1033–1041. https://doi.org/10.1002/2016JD025532

Blakeslee, R. J., H. J. Christian, M.F. Stewart, D.M. Mach, M. Bateman, T.D. Walker, et al., 2014: Lightning Imaging Sensor (LIS) for the International Space Station (ICC): Mission description and science goals, *XV Int. Conf. Atmos. Electricity*. Norman, OK, 15 pp.

Blakeslee, Richard J., 1998. Lightning Imaging Sensor (LIS) on TRMM science data. Dataset available online from the NASA Global Hydrology Center DAAC, Huntsville, Alabama, U.S.A. DOI: http://doi.org/10.5067/LIS/LIS/DATA201.

Blakeslee, Richard J., 2017. NRT Lightning Imaging Sensor (LIS) on International Space Station (ISS) provisional science data. Dataset available online from the NASA Global Hydrology Center DAAC, Huntsville, Alabama, U.S.A. DOI: http://doi.org/10.5067/LIS/ISSLIS/DATA205

Blanc, E., Farges, T., Brebion, D., An, N., Belyaev, V. V., Alpatov, A. L., & Melnikov, V. (2007). Main results of LSO (Lightning and sprite observations) on board of the International Space Station. *Microgravity Science and Technology*, *19*(5-6), 80–84. https://doi.org/10.1007/BF02919458

Boccippio, D., Goodman, S., & Heckman, S. (2000). Regional differences in tropical lightning distributions. *Journal of Applied Meteorology*, *39*(12), 2231–2248. https://doi.org/10.1175/1520-0450(2001)040<2231:RDITLD>2.0.CO;2

Boccippio, D. J., Koshak, W., Blakeslee, R., Driscoll, K., Mach, D., Buechler, D., et al. (2000). The Optical Transient Detector (OTD): Instrument characteristics and cross-sensor validation. *Journal of Atmospheric and Oceanic Technology*, *17*(4), 441–458. https://doi.org/10.1175/1520-0426(2000)017<0441:TOTDOI>2.0.CO;2

Boccippio, D. J., Koshak, W. J., & Blakeslee, R. J. (2002). Performance assessment of the Optical Transient Detector and Lightning Imaging Sensor. Part I: Predicted diurnal variability. *Journal of Atmospheric and Oceanic Technology*, *19*, 1318–1332. https://doi.org/10.1175/1520-0426(2002)019<1318:PAOTOT>2.0.CO;2

Boggs, L. D., Liu, N., Peterson, M., Lazarus, S., Splitt, M., Lucena, F., et al. (2019). First observations of gigantic jets from geostationary orbit. *Geophysical Research Letters*, *46*, 3999–4006. https://doi.org/10.1029/2019GL082278

Bruning, E. C., & MacGorman, D. R. (2013). Theory and observations of controls on lightning flash size spectra. *Journal of the Atmospheric Sciences*, *70*, 4012–4029. https://doi.org/10.1175/JAS-D-12-0289.1

Bruning, E. C., Weiss, S. A., & Calhoun, K. M. (2014). Continuous variability in thunderstorm primary electrification and an evaluation of inverted-polarity terminology. *Atmospheric Research*, *135-136*, 274–284. https://doi.org/10.1016/j.atmosres.2012.10.009

Byers, H. R., & Braham, R. R. (1949). *The thunderstorm: Report of the Thunderstorm Project*. Washington, DC: US Government Printing Office.

Carey, L. D., Murphy, M. J., McCormick, T. L., & Demetriades, N. W. S. (2005). Lightning location relative to storm structure in a leading-line, trailing-stratiform mesoscale convective system. *Journal of Geophysical Research*, *110*, D03105. https://doi.org/10.1029/2003JD004371

Cecil, D. J., Buechler, D. E., & Blakeslee, R. J. (2014). Gridded lightning climatology from TRMM-LIS and OTD: Dataset description. *Atmospheric Research*, *135-136*, 404–414. https://doi.org/10.1016/j.atmosres.2012.06.028

Cecil, D. J., Buechler, D. E., & Blakeslee, R. J. (2015). TRMM LIS climatology of thunderstorm occurrence and conditional lightning flash rates. *Journal of Climate*, *28*(16), 6536–6547. https://doi.org/10.1175/JCLI-D-15-0124.1

Cecil, D. J., Goodman, S. J., Boccippio, D. J., Zipser, E. J., & Nesbitt, S. W. (2005). Three years of TRMM precipitation features. Part I: Radar, Radiometric, and Lightning Characteristics. *Monthly Weather Review*, *133*(3), 543–566. https://doi.org/10.1175/MWR-2876.1

Christian, H. J., Blakeslee, R. J., Boccippio, D. J., Boeck, W. L., Buechler, D. E., Driscoll, K. T., et al. (2003). Global frequency and distribution of lightning as observed from space by the Optical Transient Detector. *Journal of Geophysical Research*, *108*(D1), 4005. https://doi.org/10.1029/2002JD002347

Christian, H. J., Blakeslee, R. J., & Goodman, S. J. (1989). The detection of lightning from geostationary orbit. *Journal of Geophysical Research*, *94*(D11), 13,329–13,337. https://doi.org/10.1029/JD094iD11p13329

Christian, H. J., Blakeslee, R. J., Goodman, S. J., & Mach, D. M. (Eds) (2000). *Algorithm Theoretical Basis Document (ATBD) for the Lightning Imaging Sensor (LIS)*. Alabama. (Available as: NASA/Marshall Space Flight Center. http://eospso.gsfc.nasa.gov/atbd/listables.html posted 1 Feb. 2000

Christian, H. J., & Goodman, S. J. (1987). Optical observations of lightning from a high altitude airplane. *Journal of Atmospheric and Oceanic Technology*, *4*(4), 701–711. https://doi.org/10.1175/1520-0426(1987)004<0701:OOOLFA>2.0.CO;2

Coleman, L. M., Stolzenburg, M., Marshall, T. C., & Stanley, M. (2008). Horizontal lightning propagation, preliminary breakdown, and electric potential in New Mexico thunderstorms. *Journal of Geophysical Research: Atmospheres*, *113*(D9).

Deierling, W., & Petersen, W. A. (2008). Total lightning activity as an indicator of updraft characteristics. *Journal of Geophysical Research*, *113*, D16210. https://doi.org/10.1029/2007JD009598

Deierling, W., Petersen, W. A., Latham, J., Ellis, S., & Christian, H. J. (2008). The relationship between lightning activity and ice fluxes in thunderstorms. *Journal of Geophysical Research*, *113*, D15210. https://doi.org/10.1029/2007JD009700

Ely, B. L., Orville, R. E., Lawrence, D. C., & Hodapp, C. L. (2008). Evolution of the total lightning structure in a leading-line, trailing-stratiform mesoscale convective system over Houston, Texas. *Journal of Geophysical Research*, *113*, D08114. https://doi.org/10.1029/2007JD008445

Goodman, S. J., Blakeslee, R. J., Koshak, W. J., Mach, D., Bailey, J., Buechler, D., et al. (2013). The GOES-R Geostationary Lightning Mapper (GLM). *Journal of Atmospheric Research*, *125-126*, 34–49. https://doi.org/10.1016/j.atmosres.2013.01.006

Goodman, S. J., Christian, H. J., Buechler, D. E., & Rust, W. D. (1989). A comparison of the optical pulse characteristics of intracloud and cloud-to ground lightning as observed above clouds. *Journal of Applied Meteorology*, *27*(12), 1369–1381. https://doi.org/10.1175/1520-0450(1988)027<1369:ACOTOP>2.0.CO;2

Goodman, S. J., D. Mach, W. J. Koshak, and R. J. Blakeslee, 2010: GLM Lightning Cluster-Filter Algorithm (LCFA) Algorithm Theoretical Basis Document (ATBD). NOAA NESDIS Center for Satellite Applications and Research. (Available as https://www.goes-r.gov/products/ATBDs/baseline/Lightning_v2.0_no_color.pdf, posted 24 Sept. 2010)

Jayaratne, E. R., Saunders, C. P. R., & Hallet, J. (1983). Laboratory studies of the charging of soft hail during ice crystal interactions. *Quarterly Journal of the Royal Meteorological Society*, *109*(461), 609–630. https://doi.org/10.1002/qj.49710946111

Kirkland, M. W., 1999: An examination of superbolt-class lightning events observed by the FORTE satellite. Los Alamos National Laboratory Report LA-UR-99-1685.

Koshak, W. J., Solakiewicz, R. J., Phanord, D. D., & Blakeslee, R. J. (1994). Diffusion model for lightning radiative transfer. *Journal of Geophysical Research*, *99*(D7), 14,361–14,371. https://doi.org/10.1029/94JD00022

Krehbiel, P. R. (1986). The electrical structure of thunderstorms. In *The Earth's electrical environment*, (pp. 90–113). Washington, DC: National Acad. Press.

Kuhlman, K. M., MacGorman, D. R., Biggerstaff, M. I., & Krehbiel, P. R. (2009). Lightning initiation in the anvils of two supercell storms. *Geophysical Research Letters*, *36*, L07802. https://doi.org/10.1029/2008GL036650

Kummerow, C., Barnes, W., Kozu, T., Shiue, J., & Simpson, J. (1998). The Tropical Rainfall Measuring Mission (TRMM) sensor package. *Journal of Atmospheric and Oceanic Technology*, *15*, 809–817.

Lang, T., Pédeboy, S., Rison, W., Cerveny, R., Montanyà, J., Chauzy, S., et al. (2017). WMO World Record Lightning Extremes: Longest reported flash distance and longest reported flash duration. *Bulletin of the American Meteorological Society*, *98*(6), 1153–1168. https://doi.org/10.1175/BAMS-D-16-0061.1

Lang, T. J., & Rutledge, S. A. (2008). Kinematic, microphysical, and electrical aspects of an asymmetric bow echo mesoscale convective system observed during STEPS. *Journal of Geophysical Research*, *113*, D08213. https://doi.org/10.1029/2006JD007709

Lang, T. J., Rutledge, S. A., & Wiens, K. C. (2004). Origins of positive cloud-to-ground lightning in the stratiform region of a mesoscale convective system. *Geophysical Research Letters*, *31*, L10105. https://doi.org/10.1029/2004GL019823

Light, T. E., Suszcynsky, D. M., & Jacobson, A. R. (2001). Coincident radio frequency and optical emissions from lightning, observed with the FORTE satellite. *Journal of Geophysical Research*, *106*(D22), 28,223–28,231. https://doi.org/10.1029/2001JD000727

Light, T. E., Suszcynsky, D. M., Kirkland, M. W., & Jacobson, A. R. (2001). Simulations of lightning optical waveforms as seen through clouds by satellites. *Journal of Geophysical Research*, *106*(D15), 17,103–17,114. https://doi.org/10.1029/2001JD900051

Liu, C., Zipser, E. J., Cecil, D. J., Nesbitt, S. W., & Sherwood, S. (2008). A cloud and precipitation feature database from 9 years of TRMM observations. *Journal of Applied Meteorology and Climatology*, *47*, 2712–2728. https://doi.org/10.1175/2008JAMC1890

Mach, D. M., Blakeslee, R. J., Bailey, J. C., Farrell, W. M., Goldberg, R. A., Desch, M. D., & Houser, J. G. (2005). Lightning optical pulse statistics from storm overflights during the Altus Cumulus Electrification Study. *Atmospheric Research*, *76*(1-4), 386–401. https://doi.org/10.1016/j.atmosres.2004.11.039

Mach, D. M., Christian, H. J., Blackeslee, R. J., Boccippio, D. J., Goodman, S. J., & Boeck, W. L. (2007). Performance assessment of the Optical Transient Detector and Lightning Imaging Sensor. *Journal of Geophysical Research*, *112*, D09210. https://doi.org/10.1029/2006JD007787

Mansell, E. R., MacGorman, D. R., Ziegler, C. L., & Straka, J. M. (2005). Charge structure and lightning sensitivity in a simulated multicell thunderstorm. *Journal of Geophysical Research*, *110*, D12101. https://doi.org/10.1029/2004JD005287

Marshall, T. C., & Rust, W. D. (1993). Two types of vertical electrical structures in stratiform precipitation regions of mesoscale convective systems. *Bulletin of the American Meteorological Society*, *74*(11), 2159–2170. https://doi.org/10.1175/1520-0477(1993)074<2159:TTOVES>2.0.CO;2

Marshall, T. C., Rust, W. D., Winn, W. P., & Gilbert, K. E. (1989). Electrical structure in two thunderstorm anvil clouds. *Journal of Geophysical Research*, *94*(D2), 2171–2181. https://doi.org/10.1029/JD094iD02p02171

Marshall, T. C., Stolzenburg, M., Krehbiel, P. R., Lund, N. R., & Maggio, C. R. (2009). Electrical evolution during the decay stage of New Mexico thunderstorms. *Journal of Geophysical Research*, *114*, D02209. https://doi.org/10.1029/2008JD010637

NOAA-NASA, 2019: GLM instrument description: GOES-R Series Data Book, CDRL PM-14 Rev A. May 2019, Available at. https://www.goes-r.gov/downloads/resources/documents/GOES-RSeriesDataBook.pdf

Peterson, M. (2019a). Research applications for the Geostationary Lightning Mapper (GLM) operational lightning flash data product. *Journal of Geophysical Research: Atmospheres*, *124*, 10,205–10,231. https://doi.org/10.1029/2019JD031054

Peterson, M. (2019b). Using lightning flashes to image thunderclouds. *Journal of Geophysical Research: Atmospheres*, *124*, 10,175–10,185. https://doi.org/10.1029/2019JD031055

Peterson, M., & Rudlosky, S. (2019). The time evolution of optical lightning flashes. *Journal of Geophysical Research*, *124*(1), 333–349. https://doi.org/10.1029/2018JD028741

Peterson, M., Rudlosky, S., & Deierling, W. (2018). Mapping the lateral development of lightning flashes from orbit. *Journal of Geophysical Research: Atmospheres*, *123*(17), 9674–9687. https://doi.org/10.1029/2018JD028583

Peterson, M. J., 2014: Variations of optical and radio lightning characteristics and the relationship between storm convective intensity and above-cloud electric fields, Ph.D. dissertation, 253 pages.

Peterson, M. J., Deierling, W., Liu, C., Mach, D., & Kalb, C. (2017). The properties of optical lightning flashes and the clouds they illuminate. *Journal of Geophysical Research: Atmospheres*, *122*, 423–442. https://doi.org/10.1002/2016JD025312

Peterson, M. J., & Liu, C. (2011). Global statistics of lightning in anvil and stratiform regions over the tropics and subtropics observed by TRMM. *Journal of Geophysical Research*, *116*, D23201. https://doi.org/10.1029/2011JD015908

Peterson, M. J., & Liu, C. (2013). Characteristics of lightning flashes with exceptional illuminated areas, durations, and optical powers and surrounding storm properties in the tropics and inner subtropics. *Journal of Geophysical Research: Atmospheres*, *118*, 11,727–11,740. https://doi.org/10.1002/jgrd.50715

Peterson, M. J., Rudlosky, S., & Deierling, W. (2017). The evolution and structure of extreme optical lightning flashes. *Journal of Geophysical Research: Atmospheres*, *122*, 13,370–13,386. https://doi.org/10.1002/2017JD026855

Reynolds, S. E., Brook, M., & Gourley, M. F. (1957). Thunderstorm charge separation. *Journal of Meteorology*, *14*(5), 163–178.

Rison, W., Thomas, R. J., Krehbiel, P. R., Hamlin, T., & Harlin, J. (1999). A GPS-based three-dimensional lightning mapping system: Initial observations in central New Mexico. *Geophysical Research Letters*, *26*(23), 3573–3576. https://doi.org/10.1029/1999GL010856

Rudlosky, S., S. J. Goodman, and K. S. Virts, 2020: Chapter 16 - Lightning Detection: GOES-R Series Geostationary Lightning Mapper. S. J. Goodman, T. J. Schmit, J. Daniels, R. J. Redmon (Eds.), *The GOES-R Series* (pp. 193–202). Academic Press. https://doi.org/10.1016/B978-0-12-814327-8.00016-0

Rudlosky, S. D., Goodman, S. J., Virts, K. S., & Bruning, E. C. (2018). Initial Geostationary Lightning Mapper observations. *Geophysical Research Letters*, *46*, 1097–1104. https://doi.org/10.1029/2018GL081052

Rumpf, C. M., Longenbaugh, R. S., Henze, C. E., Chavez, J. C., & Mathias, D. L. (2019). An algorithmic approach for detecting bolides with the Geostationary Lightning Mapper. *Sensors*, *19*, 1008. https://doi.org/10.3390/s19051008

Rust, W. D., MacGorman, D. R., Bruning, E. C., Weiss, S. A., Krehbiel, P. R., Thomas, R. J., et al. (2005). Inverted-polarity electrical structures in thunderstorms in the Severe Thunderstorm Electrification and Precipitation Study (STEPS). *Atmospheric Research*, *76*(1-4), 247–271. https://doi.org/10.1016/j.atmosres.2004.11.029

Saunders, C. P. R., Keith, W. D., & Mitzeva, R. P. (1991). The effect of liquid water content on thunderstorm charging. *Journal of Geophysical Research*, *96*(D6), 11,007–11,017. https://doi.org/10.1029/91JD00970

Saunders, C. P. R., & Peck, S. L. (1998). Laboratory studies of the influence of the rime accretion rate on charge transfer during crystal/graupel collisions. *Journal of Geophysical Research*, *103*(D12), 13,949–13,956. https://doi.org/10.1029/97JD02644

Schmit, T. J., Griffith, P., Gunshor, M. M., Daniels, J. M., Goodman, S. J., & Lebair, W. J. (2017). A closer look at the ABI on GOES-R. *Bulletin of the American Meteorological Society*, *98*(4), 681–698. https://doi.org/10.1175/BAMS-D-15-00230.1

Schmit, T. J., Lindstrom, S. S., Gerth, J. J., & Gunshor, M. M. (2018). Applications of the 16 spectral bands on the Advanced Baseline Imager (ABI). *Journal of Operational Meteorology*, *6*(4), 33–46. https://doi.org/10.15191/nwajom.2018.0604

Schultz, C. J., Carey, L. D., Schultz, E. V., & Blakeslee, R. J. (2017). Kinematic and microphysical significance of lightning jumps versus nonjump increases in total flash rate. *Weather and Forecasting*, *32*(1), 275–288. https://doi.org/10.1175/WAF-D-15-0175.1

Schultz, C. J., Peterson, W. A., & Carey, L. D. (2009). Preliminary development and evaluation of lightning jump algorithms for real-time detection of severe weather. *Journal of Applied Meteorology and Climatology*, *48*(12), 2543–2563. https://doi.org/10.1175/2009JAMC2237.1

Stolzenburg, M., Marshall, T. C., Rust, W. D., & Smull, B. F. (1994). Horizontal distribution of electrical and meteorological conditions across the stratiform region of a mesoscale convective system. *Monthly Weather Review*, *122*(8), 1777–1797. https://doi.org/10.1175/1520-0493(1994)122<1777:HDOEAM>2.0.CO;2

Stolzenburg, M., Rust, W. D., Smull, B. F., & Marshall, T. C. (1998). Electrical structure in thunderstorm convective regions: 1. Mesoscale convective systems. *Journal of Geophysical Research*, *103*(D12), 14,059–14,078. https://doi.org/10.1029/97JD03546

Takahashi, T. (1978). Riming electrification as a charge generation mechanism in thunderstorms. *Journal of the Atmospheric Sciences*, *35*(8), 1536–1548. https://doi.org/10.1175/1520-0469(1978)035<1536:REAACG>2.0.CO;2

Takahashi, T., & Miyawaki, K. (2002). Reexamination of riming electrification in a wind tunnel. *Journal of the Atmospheric Sciences*, *59*(5), 1018–1025. https://doi.org/10.1175/1520-0469(2002)059<1018:ROREIA>2.0.CO;2

Thomas, R., Krehbiel, P. R., Rison, W., Hamlin, T., Boccippio, D. J., Goodman, S. J., & Christian, H. J. (2000). Comparison of ground-based 3-dimensional lightning mapping observations with satellite-based LIS observations in Oklahoma. *Geophysical Research Letters*, *27*(12), 1703–1706. https://doi.org/10.1029/1999GL010845

Thomson, L. W., & Krider, E. P. (1982). The effects of clouds on the light produced by lightning. *Journal of the Atmospheric Sciences*, *39*, 2051–2065. https://doi.org/10.1175/1520-0469(1982)039<2051:TEOCOT>2.0.CO;2

Turman, B. N. (1977). Detection of lightning superbolts. *Journal of Geophysical Research*, *82*(18), 2566–2568. https://doi.org/10.1029/JC082i018p02566

Uman, M. A. (1978). Criticism of "Comment on 'Detection of lightning superbolts' by B. N. Turman" by R. D. Hill. *Journal of Geophysical Research*, *83*(C11), 5523–5523. https://doi.org/10.1029/JC083iC11p05523

Vonnegut, B., Vaughan, O. H., Brook, M., & Krehbiel, P. (1985). Mesoscale observations of lightning from Space Shuttle. *Bulletin of the American Meteorological Society*, *66*(1), 20–29. https://doi.org/10.1175/1520-0477(1985)066<0020:MOOLFS>2.0.CO;2

Weiss, S. A., MacGorman, D. R., & Calhoun, K. M. (2012). Lightning in the anvils of supercell thunderstorms. *Monthly Weather Review*, *140*(7), 2064–2079. https://doi.org/10.1175/MWR-D-11-00312.1

Williams, E. R. (1989). The tripole structure of thunderstorms. *Journal of Geophysical Research*, *94*(D11), 13,151–13,167. https://doi.org/10.1029/JD094iD11p13151

Winn, W. P., Aulich, G. D., Hunyady, S. J., Eack, K. B., Edens, H. E., Krehbiel, P. R., et al. (2011). Lightning leader stepping, K changes, and other observations near an intracloud flash. *Journal of Geophysical Research*, *116*, D23115. https://doi.org/10.1029/2011JD015998

Zipser, E. J., Cecil, D. J., Liu, C., Nesbitt, S. W., & Yorty, D. P. (2006). Where are the most intense thunderstorms on Earth? *Bulletin of the American Meteorological Society*, *87*(8), 1057–1072. https://doi.org/10.1175/BAMS-87-8-1057